

STRUCTURAL AND OPTOELECTRONIC PROPERTIES OF VANADIUM
PENTOXIDE THIN FILMS DEPOSITED BY ULTRASONIC SPRAY
PYROLYSIS

A THESIS SUBMITTED TO
THE GRADUATE SCHOOL OF NATURAL AND APPLIED SCIENCES
OF
MIDDLE EAST TECHNICAL UNIVERSITY

BY

ŞEYMA KOÇ

IN PARTIAL FULFILLMENT OF THE REQUIREMENTS
FOR
THE DEGREE OF MASTER OF SCIENCE
IN
METALLURGICAL AND MATERIALS ENGINEERING

DECEMBER 2019

Approval of the thesis:

**STRUCTURAL AND OPTOELECTRONIC PROPERTIES OF VANADIUM
PENTOXIDE THIN FILMS DEPOSITED BY ULTRASONIC SPRAY
PYROLYSIS**

submitted by **ŞEYMA KOÇ** in partial fulfillment of the requirements for the degree
of **Master of Science in Metallurgical and Materials Engineering Department,**
Middle East Technical University by,

Prof. Dr. Halil Kalıpçılar
Dean, Graduate School of **Natural and Applied Sciences**

Prof. Dr. Cemil Hakan Gür
Head of Department, **Met. and Mat. Eng., METU**

Prof. Dr. Hüsnu Emrah Ünalın
Supervisor, **Met. and Mat. Eng., METU**

Assist. Prof. Dr. Simge Çınar
Co-Supervisor, **Met. and Mat. Eng., METU**

Examining Committee Members:

Assoc. Prof. Dr. Emrullah Görkem Günbaş
Chemistry, METU

Prof. Dr. Hüsnu Emrah Ünalın
Met. and Mat. Eng., METU

Assist. Prof. Dr. Simge Çınar
Met. and Mat. Eng., METU

Assist. Prof. Dr. Selçuk Yerci
Micro and Nanotechnology, METU

Assist. Prof. Dr. Şahin Coşkun
Met. and Mat. Eng., ESOGÜ

Date: 13.12.2019

I hereby declare that all information in this document has been obtained and presented in accordance with academic rules and ethical conduct. I also declare that, as required by these rules and conduct, I have fully cited and referenced all material and results that are not original to this work.

Name, Surname: Şeyma Koç

Signature:

ABSTRACT

STRUCTURAL AND OPTOELECTRONIC PROPERTIES OF VANADIUM PENTOXIDE THIN FILMS DEPOSITED BY ULTRASONIC SPRAY PYROLYSIS

Koç, Şeyma

Master of Science, Metallurgical and Materials Engineering

Supervisor: Prof. Dr. Hüsnü Emrah Ünalın

Co-Supervisor: Assist. Prof. Dr. Simge Çınar

December 2019, 77 pages

Nanocrystalline vanadium pentoxide (V_2O_5) thin films were deposited onto fluorine doped tin oxide (FTO) coated glass substrates using ultrasonic spray pyrolysis and spin coating methods. The formation behavior of thin films, the effects of different production methods on the characteristics of the films and their microstructural / physical properties were investigated as a function of annealing temperature in the range of 450-550 °C and other controllable process parameters.

Structural, morphological and optoelectronic properties of orthorhombic V_2O_5 films were examined by X-Ray diffraction, Raman spectroscopy, X-Ray photoelectron spectroscopy, scanning electron microscope, atomic force microscopy, UV-VIS spectroscopy and CV measurements. It was clear that homogeneous thin films were obtained in a reproducible manner through ultrasonic spray deposition. Particle size of the films was found to increase with the annealing temperature. Optical transmittance of the films got adversely affected as the roughness increased. All heat treated films showed electrochromic (EC) response and for films with a thickness of 50 nm, the transmittance change was about %10 at a wavelength of 800 nm. Ultrasonic spray deposition method was utilized as a reproducible and cost-effective method.

Parametric optimization approach represented herein this thesis for the ultrasonic spray deposition of V_2O_5 thin films can be easily applied to other oxide systems.

Keywords: Thin Film Deposition, Ultrasonic Spray Pyrolysis, Vanadium Pentoxide, Electrochromics.

ÖZ

ULTRASONİK SPREY KAPLAMA YÖNTEMİ İLE ÜRETİLEN VANADYUM PENTOKSİT İNCE FİMLERİNİN YAPISAL VE OPTOELEKTRONİK ÖZELLİKLERİNİN İNCELENMESİ

Koç, Şeyma
Yüksek Lisans, Metalurji ve Malzeme Mühendisliği
Tez Danışmanı: Prof. Dr. Hüsnü Emrah Ünalın
Ortak Tez Danışmanı: Dr. Öğr. Üyesi Simge Çınar

Aralık 2019, 77 sayfa

[Nanokristal vanadyum pentoksit (V_2O_5) ince filmler, flor katkılı kalay oksit (FTO) kaplı cam yüzeyler üzerine ultrasonik sprej kaplama ve döndürme yöntemleri kullanılarak kaplanmıştır. Üretilen ince filmlerin oluşum davranışları, farklı üretim yöntemlerinin filmlerin özellikleri üzerine etkileri ve mikroyapısal-fiziksel özelliklerin $450-550$ ° C aralığında uygulanan ısı işleme göre değişimleri incelenmiştir.

V_2O_5 filmlerin yapısal, morfolojik ve optoelektronik özellikleri X-ışını difraksiyonu, Raman spektroskopisi, X-ışını fotoelektron spektroskopisi, taramalı elektron mikroskobu, atomik kuvvet mikroskobu, UV-VIS spektroskopisi ve CV ölçümleri ile incelenmiştir. Homojen ince filmlerin, ultrasonik sprej kaplama yoluyla tekrarlanabilir bir şekilde elde edildiği görülmüştür. Ayrıca, filmlerin partikül büyüklüğünün tavlama sıcaklığı ile arttığı bulunmuştur. Pürüzlülük arttıkça filmlerin optik geçirgenliği olumsuz etkilenmiştir. Isıl işlem uygulanan tüm filmler elektrokromik tepki sergilemiş ve 50 nm kalınlığa sahip olan bu filmler için optik geçirgenlik değişimi 800 nm dalga boyunda yaklaşık % 10'dur. Bu tezde, ultrasonik sprej kaplama yöntemi tekrarlanabilir ve düşük maliyetli bir yöntem olarak

kullanılmıřtır. Ultrasonik sprej kaplama yntemiyle V₂O₅ ince filmlerinin elde edilmesi iin kullanılan parametrik optimizasyon yaklařımı, diđer oksit sistemlerine kolayca uygulanabilir.

Anahtar Kelimeler: İnce Film Kaplama, Ultrasonik Sprej Kaplama, Vanadyum Pentoksit, Elektrokromizm

To my family...

ACKNOWLEDGEMENTS

First of all, I would like to express my sincere gratitude to my advisor Prof. Dr. Hüsni Emrah Ünalın, for his great support, wise guidance and patience. Working under his supervision is a source of great honor throughout all my studies.

I extend my sincere thanks to my savior friend Yusuf Tutel, Serkan Koylan and Mete Batuhan Durukan. I am grateful to you for encouraging me to complete this work and for giving me all support.

I also owe my gratitude Assoc. Prof. Dr. Emrah Özensoy, his team at Bilkent University and specially Dr. Farzaneh Hekmat for their help. Their valuable comments contributed greatly to my thesis.

I would like to thank you Prof. Dr. İshak Karakaya and Dr. Mustafa Aras for their valuable help.

I owe great gratitude to my labmates and my dearest friends Doğa Doğanay, Alptekin Aydınlı, Doğançan Tıgan, Selin Özkul, Can Çuhadar, Şensu Tunca, Merve Nur Güven, Elif Güner and Onur Türel for their support and friendship.

I would also like to thank you my dear colleagues, Deniz Ceran, Utku Burgaz, Özgür Polat, Hasan Umut Gacal, Sinan Öztürk and Uğur Kahraman for the great emotional support with their special techniques.

I would like to thank my dear friends, Melih Öztürk, Aslıhan Yıldız, Kevser Atmaca, Kağan Yıldız, Görkem Özer, Gözden Torun, Bilge Çilingir, Selen Yüksel and Aslıhan Alpaslan for always being with me.

My special thanks go to my lovely friend Tansu Yılmaz and Gizem Küçüklergil. I would not have achieved this goal without your endless support.

Finally, I must present my deepest thanks to my loved ones. My dear family and dear darling! Endless thanks for being there and supporting me whenever I need it.

TABLE OF CONTENTS

ABSTRACT	v
ÖZ.....	vii
ACKNOWLEDGEMENTS	x
TABLE OF CONTENTS.....	xii
LIST OF TABLES.....	xv
LIST OF FIGURES	xvi
LIST OF ABBREVIATIONS	xix
CHAPTERS	
1. INTRODUCTION	1
1.1. Deposition Techniques for V ₂ O ₅ Thin Films	1
1.1.1. Physical Methods	3
1.1.2. Chemical Process	3
1.1.2.1. Dip-Coating.....	3
1.1.2.2. Spin Coating.....	4
1.1.2.3. Spray Pyrolysis.....	5
1.1.2.3.1 Effects of Deposition Parameters on Film Properties.....	6
1.1.2.3.2 Thin Film Deposition Models by Spray Pyrolysis	8
1.1.2.3.2.1 Atomization of Precursor Solution	8
1.1.2.3.2.2 Aerosol Transport	10
1.2. Characterizations of V ₂ O ₅ Thin Films.....	13
1.2.1. Structure and Morphology.....	13
1.2.2. Optical Properties.....	18
1.2.3. Electrical Properties	20

1.3. Applications of V ₂ O ₅ Thin Films	23
1.3.1. Supercapacitors	23
1.3.2. Gas Sensors.....	23
1.3.3. Electrochromic Devices	25
1.3.4. Solar Cells.....	27
1.3.5. Li Microbatteries.....	31
2. MATERIALS AND METHODS	35
2.1. Materials	35
2.2. Experimental Procedure.....	35
2.2.1. Cleaning Procedure of Glass Substrates.....	35
2.2.2. Preparation of Coating Solution.....	35
2.2.3. Deposition of V ₂ O ₅ Thin Films by Spin Coating.....	36
2.2.4. Deposition of V ₂ O ₅ Thin Films by Ultrasonic Spray Coating.....	36
2.2.4.1. Ultrasonic Spray Pyrolysis System.....	36
2.2.4.2. Deposition by Sono-Tek Exacta Coat System	38
2.2.4.3. Optimization of Spray Pyrolysis System	39
2.3. Characterization of Materials	41
2.3.1. X-Ray Diffraction (XRD).....	41
2.3.2. X-Ray Photoelectron Spectroscopy (XPS).....	42
2.3.3. Raman Spectroscopy	42
2.3.4. Scanning Electron Microscopy (SEM)	42
2.3.5. Atomic Force Microscopy (AFM)	42
2.3.6. X-Ray Fluorescence (XRF)	42
2.3.7. UV-Vis Spectrophotometry	43

2.3.8. Cyclic Voltammetry	43
3. RESULTS AND DISCUSSION.....	45
3.1. X-Ray Diffraction (XRD)	45
3.2. Raman Spectroscopy	47
3.3. X-Ray Photoelectron Spectroscopy (XPS)	49
3.4. Scanning Electron Microscopy (SEM).....	51
3.5. Atomic Force Microscopy (AFM).....	53
3.6. X-Ray Fluorescence (XRF)	57
3.7. UV-Vis Spectrophotometry	58
3.8 Cyclic Voltammetry	63
4. CONCLUSIONS AND FUTURE RECOMMENDATIONS	65
REFERENCES	67

LIST OF TABLES

Table 1. 1 Characteristics of atomizers	8
Table 1. 2 Atomic positions in orthorhombic V ₂ O ₅ (space group Pmmn).....	14
Table 2. 1 List of chemicals used for the preparation V ₂ O ₅ sol	35
Table 2. 2 Designations and descriptions of the samples deposited by spin coating.	38
Table 2. 3 Parameters of ultrasonic spray pyrolysis system	39
Table 2. 4 Designations and descriptions of the samples deposited by spray pyrolysis.....	39
Table 2. 5 Summary of optimized USP parameters.....	39
Table 3. 1 XPS fit parameters for the V2p _{3/2} and O1s peaks for vanadium oxide standards (Exp.*) and values reported in literature.	50
Table 3. 2 R _a (average roughness), RMS (root mean square roughness) and average grain size values of each film.	57
Table 3. 3 Thickness of the samples measured through XRF method.	58

LIST OF FIGURES

Figure 1. 1 Thin film deposition techniques	2
Figure 1. 2 Schematics showing steps of dip-coating	4
Figure 1. 3 Schematic of spin coating method	5
Figure 1. 4 Schematic representation of spray pyrolysis system.....	6
Figure 1. 5 Illustration of cone-jet and multi-jet modes	9
Figure 1. 6 Schematic of aerosol transport mechanism	11
Figure 1. 7 Decomposition processes with increasing temperature	12
Figure 1. 8 Crystal structure of orthorhombic V ₂ O ₅ . Views from (a) ac plane and (b) ab plane. V atoms are shown in yellow and O atoms are in blue	13
Figure 1. 9 X-ray diffraction spectra of V ₂ O ₅ films as a function of the oxygen partial pressure in the chamber deposition.....	15
Figure 1. 10 AFM images of the V ₂ O ₅ films at (a) room temperature, (b) room temperature with a smaller scan area,(c) post-annealed film deposited at room temperature, (d) 300 °C and (e) 500 °C	16
Figure 1. 11 SEM images of V ₂ O ₅ thin films prepared from (a) freshly prepared, (b) 48 h, (c) 96 h, (d) 144 h and (e) 192 h aged sol.....	17
Figure 1. 12 Optical transmittance spectra of V ₂ O ₅ films formed at substrate temperature (a) smaller than 503 K and (b)larger than 503K	19
Figure 1. 13 (a) Plots of σT vs. $1/T$ for flash-evaporated V ₂ O ₅ films obtained in various conditions. (1) as-deposited at $T_s = 25$ °C, (2) as-deposited at $T_s = 250$ °C, (3) grown at $T_s = 25$ °C and annealed in O ₂ , (4) grown at $T_s = 25$ °C and annealed in Ar, (5) grown at $T_s = 250$ °C and annealed in O ₂ and (6) grown at $T_s = 250$ °C and annealed in Ar. The annealing treatment was carried out at 300 °C for 48 h. (b) Plots of σRT and Wh vs. T_s	22
Figure 1. 14 Response of V ₂ O ₅ films prepared by spray pyrolysis at a substrate temperature of 300 °C for different VOCs vapors at a concentration of 100 ppm....	24
Figure 1. 15 Electrochromic device design, showing the movement of ions under an externally applied electric field	25

Figure 1. 16 (a) Device structure of rubrene/C ₇₀ -based OSCs and (b) respective energy band gap diagram.....	27
Figure 1. 17 The J-V characteristics of OSC devices with and without V ₂ O ₅ hole extraction layer	28
Figure 1. 18 (a) The device structure diagram. (b) J–V curves of PEDOT and PVO devices.....	29
Figure 1. 19 The (a) incident photon to electron efficiency (IPCE) spectra and (b) J–V curves obtained for the PSCs with and without V ₂ O ₅ and Bphen modified layers.	30
Figure 1. 20 Line charts that show the variation in the performance parameter of the four kinds PSCs with time including the (a) PCE, (b) V _{OC} , (c) J _{SC} and (d) FF.....	31
Figure 1. 21 Schematic cross-section of a thin-film lithium microbattery	32
Figure 2. 1 Cross-section of ultrasonic nozzle (a) and schematic representation of Vortex type	37
Figure 2. 2 Deposition path used in ultrasonic spray pyrolysis system.....	41
Figure 3. 1 . XRD patterns of spin coated V ₂ O ₅ films prepared at different annealing temperatures (a) as-deposited at room temperature, (b) 450 °C, (c) 500 °C and (d) 550 °C.	46
Figure 3. 2 XRD patterns of ultrasonic spray deposited V ₂ O ₅ films prepared at different annealing temperatures (a) as-deposited at 100 °C, (b) 450 °C, (c) 500 °C and (d) 550 °C.	46
Figure 3. 3 Raman spectra of V ₂ O ₅ thin films deposited by spin coating and ultrasonic spray pyrolysis methods.	48
Figure 3. 4 Survey spectra of USD-450 sample. Insert shows C1s.....	49
Figure 3. 5 XPS spectra for (a) O 1s and (b) V2p and core levels of the USD-450 sample.	50
Figure 3. 6 Top view SEM micrographs of SP-B with different magnification (a) 120 000, (b) 15 000 and USD-B with different magnification (c) 120 000, (d) 15 000..	51

Figure 3. 7 Top view SEM micrographs of SP-450 with different magnification (a) 120 000, (b) 15 000, SP-500 with different magnification (c) 120 000, (d) 15 000 and SP-550 with different magnification (e) 120 000, (f) 15 000.....	52
Figure 3. 8 Top view SEM micrographs of USD-450 with different magnification (a) 120 000, (b) 15 000, USD-500 with different magnification (c) 120 000, (d) 15 000 and USD-550 with different magnification (e) 120 000, (f) 15 000.....	52
Figure 3. 9 Topographical AFM 3D images of the (a) SP-B, (c) USD-B samples and 2D images of the (b) SP-B, (d) USD-B samples.	53
Figure 3. 10 Topographical AFM 3D images of the (a) SP-450, (c) USD-450 samples and 2D images of the (b) SP-450, (d) USD-450 samples.	54
Figure 3. 11 Topographical AFM 3D images of the (a) SP-500, (c) USD-500 samples and 2D images of the (b) SP-500, (d) USD-500 samples	55
Figure 3. 12 Topographical AFM 3D images of the (a) SP-500, (c) USD-500 samples and 2D images of the (b) SP-500, (d) USD-500 samples.	56
Figure 3. 13 Transmittance spectra for V ₂ O ₅ thin films deposited by (a) spin coating method and (b) USD method.....	59
Figure 3. 14 Tauc plots for (a) spin coated and (b) USD deposited V ₂ O ₅ thin films annealed at 450, 500 and 550 °C.	60
Figure 3. 15 Transmittance spectra for (a) USD-B, (b) USD-450, (c) USD-500 and (d) USD-550 samples in colored and bleached states.	61
Figure 3. 16 CV results of (a) SP-450 and (b) USD-450 samples.....	62
Figure 3. 17 CV result of the PMMA coated USD-450 sample. Inserts show the photographs of the colored thin films at respective potentials	63

LIST OF ABBREVIATIONS

AFM	Atomic Force Microscopy
CVD	Chemical Vapor Deposition
FTO	Fluorine Doped Indium Tin Oxide
MIT	Metal-to-Insulator Transition
SEM	Scanning Electron Microscope
TMO	Transition Metal Oxide
USP	Ultrasonic Spray Pyrolysis
XRD	X-ray Diffraction
XRF	X-ray Fluorescence

CHAPTER 1

INTRODUCTION

1.1. Deposition Techniques for V₂O₅ Thin Films

A coating on a certain substrate or surface with a thickness from several nanometers to a micron is called as a thin film. Films can also have atomic thickness and can be layered [1].

Thin film technology is used to modify optical and electrical properties of the substrates. Therefore, although there have been studies on thin film technology for a long time, especially with the development of nanomaterials in the late 20st century, they have received significant interest. Because, nanocrystalline thin film materials promise many advanced properties like higher conductivity and superior diffusivity [2].

Thin films may not be affected by classical metallurgical phase diagrams. Depending on the deposition conditions, their basic properties such as crystal structure, thickness, film composition, orientation and surface morphology can be arranged [3].

Choosing proper technique is very important to achieve thin films with desired properties. Same material can offer customized properties for different applications. The combination of nanomaterials and appropriate coating conditions requires the development of different deposition techniques. These deposition methods can be classified into two main groups as physical and chemical methods. These deposition methods with their subgroups can be seen in Figure 1. 1 .

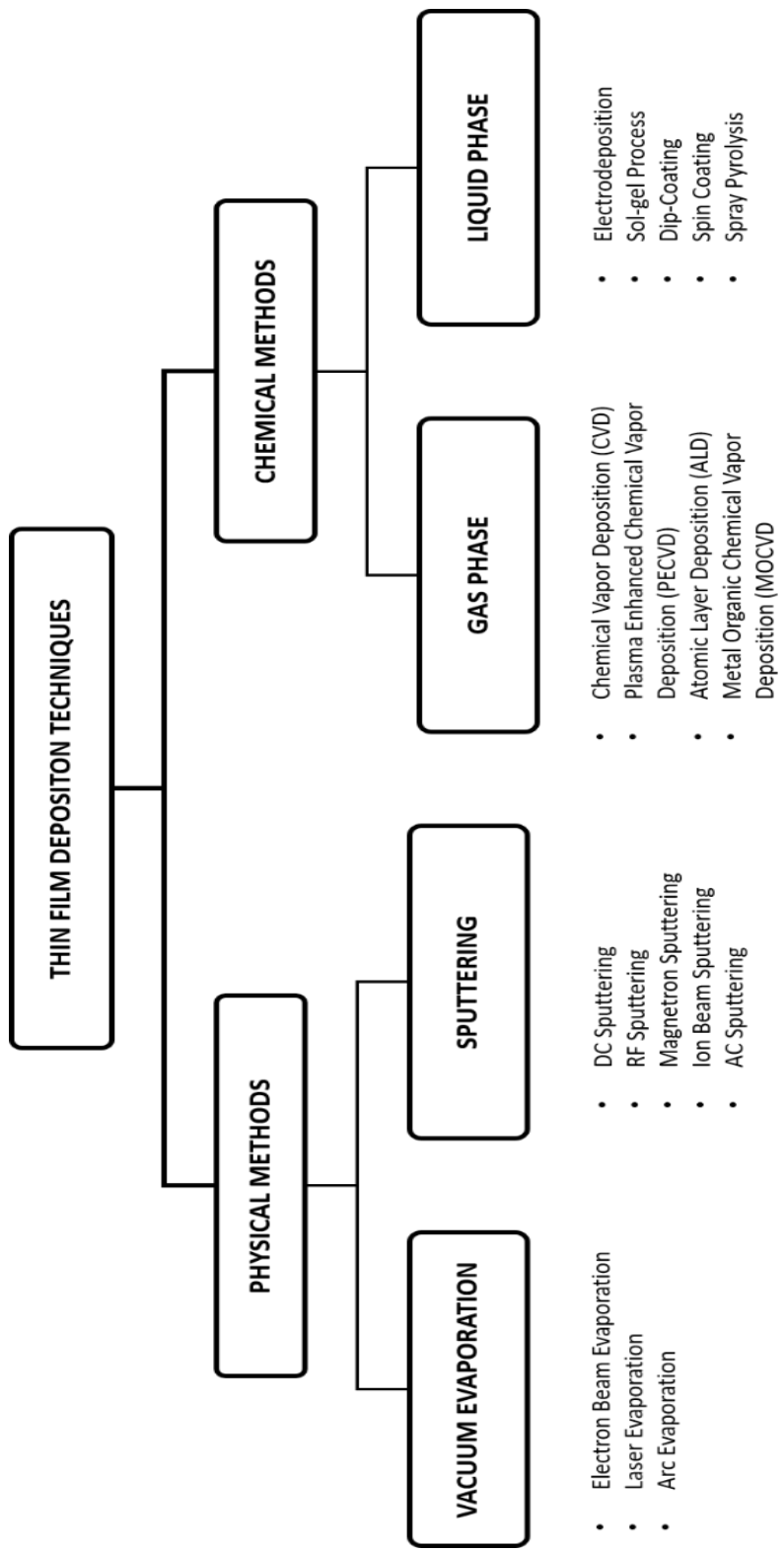


Figure 1. 1 Thin film deposition techniques.

1.1.1. Physical Methods

In principle, electromechanical or mechanical techniques are used in physical processes. These methods include evaporation and sputtering. Thin film formation consists of two main ways: evaporation and transformation of the gaseous material [4].

Thermal evaporation (arc, laser, and electron beam), sputtering (DC, RF, AC, Magnetron) and ion plating are different types of physical methods [4].

Although high quality thin films can be produced using physical techniques, these methods have disadvantages that cannot be excluded. Limited deposition area, requirement of complex instruments, waste of coating material and cost of the system are just some of these drawbacks including vacuum requirements. These disadvantages have encouraged researchers to explore chemical methods that are easier and less costly.

1.1.2. Chemical Process

Sol gel is one of the most commonly used chemical process for the deposition of thin films. It can be used for the fabrication of various materials such as nanocomposites, inorganics and hybrids. This method allows for more control of key features. It provides flexibility to be applied to different substrates and complex geometries. There are several routes of liquid phase based chemical methods. Dip coating, spin coating and spray pyrolysis can be given as most important techniques [5].

1.1.2.1. Dip-Coating

Dip coating is one of the wet thin film deposition methods which is practiced humidity and temperature. Schematic showing sequential steps of dip coating is shown in Figure 1. 2. In its simplest form, the coating process begins by dipping the substrate into the precursor solution and proceeding at a constant rate of withdrawal. The control of evaporation conditions and withdrawal speed makes it possible to adjust the thin film properties. These properties can be listed as thickness, morphology, optical properties,

structure etc. The solution is distributed homogeneously on the substrate surface under the effect of viscous drag and capillary action. The final stage of the coating is the evaporation process, which enables film gelation. Generally, to obtain desired properties of thin film a post-heat treatment is applied [6].

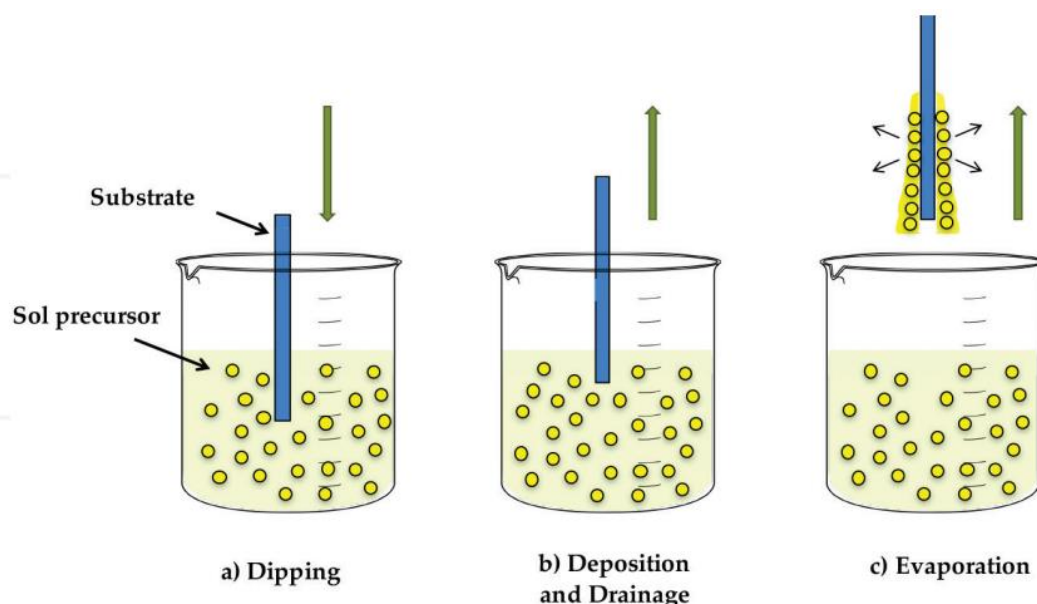


Figure 1. 2 Schematics showing steps of dip-coating [6].

1.1.2.2. Spin Coating

Spin coating is another simple chemical deposition method for the deposition of thin and homogeneous films. This process is based on the application of a liquid solution to a rotating substrate which is perpendicular to the spin axis. Spin coating consists of 4 basic step, which are deposition, spin-up, spin-off and evaporation. These stages are schematically shown in Figure 1. 3 . In deposition stage, precursor solution is loaded onto a rotating substrate. Viscosity of the solution and the size of the coating area determines the required amount of liquid. The applied solution spreads to the substrate surface under the influence of centrifugal force during spin up. Depending on the desired film thickness, spinning speed is arranged. Then, the coated surface is usually rotated at a higher speed to remove the excessive liquid which is spread towards and eventually out of the edges. The evaporation stage is manifested in the final stage as

the basis of the thinning mechanism. Type of the solvent and substrate, concentration of precursor solution, spinning speed and substrate temperature play a key role in determining the thickness and quality of the thin film. Thin films with a highly uniform thickness can be easily deposited through optimizing the spin speed and viscosity of the solution. However, in this method, the size of the substrate to be coated is a limiting factor since large substrates cannot be rotated with high speeds [7][8].

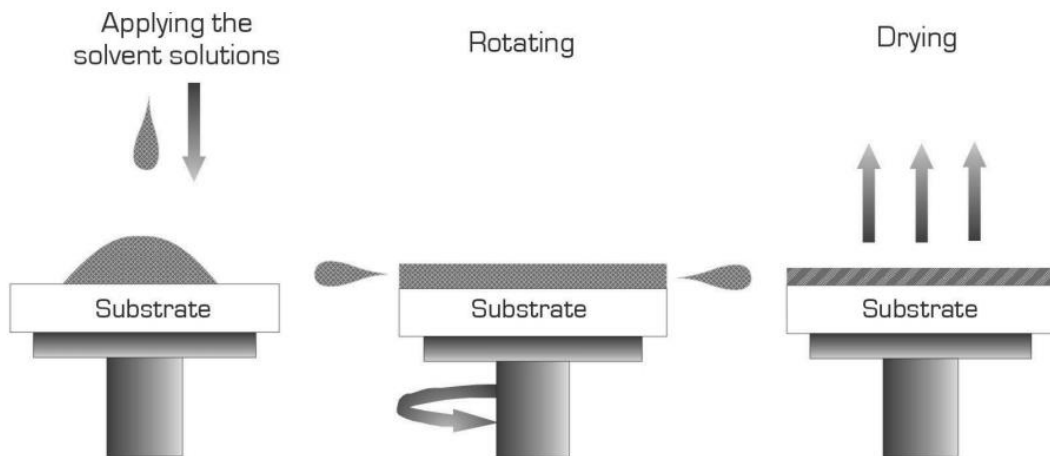


Figure 1. 3 Schematic of spin coating method [8].

1.1.2.3. Spray Pyrolysis

Spray pyrolysis is a well-known technique for the formation of thick and thin films, powders and ceramic coatings. In contrast to other thin film coating techniques, it is highly preferred since it is a very simple and particularly affordable method in terms of equipment cost. Desired films with unique composition can easily be obtained. This method is applied to deposit porous films, dense films, even multilayered films. Powders can also be formed using spray pyrolysis. Spray pyrolysis has been studied for the last 3 decades in different fields like microelectronics, optoelectronics, microbatteries and electrochromic devices, thermochromic devices and solar cells. [9]

Spray pyrolysis systems typically include a precursor solution, atomizer, substrate heater and controller of temperature and pressure. Air blast (solution undergoes an air

stream), ultrasonic (short wavelengths for required atomization are created by ultrasonic frequencies) and electrostatic (solution is exposed to electric field) are the different types of atomizers used in this method.

1.1.2.3.1 Effects of Deposition Parameters on Film Properties

In the spray pyrolysis method, precursor solution made up of solute and solvent is sprayed onto a heated substrate. Liquids such as distilled water, ethanol, isopropanol are typically used as solvents. Inorganic and organic compounds are used as solute materials. A schematic of the spray pyrolysis system is provided in Figure 1. 4.

When metal salts are chosen as the solute material in the precursor solution, drops of liquid strike the substrate surface, spread out in the form of a disc and undergo thermal decomposition. Especially depending on the substrate temperature, volume and momentum of droplets, droplet's shape and size are altered. At the end of the process, thin film is obtained by overlapping these disks of metal salts transformed into oxides on the substrate. This process is influenced by several parameters that affect the structure and properties of the coated film. Temperature and precursor solution type are the two most important parameters [10].

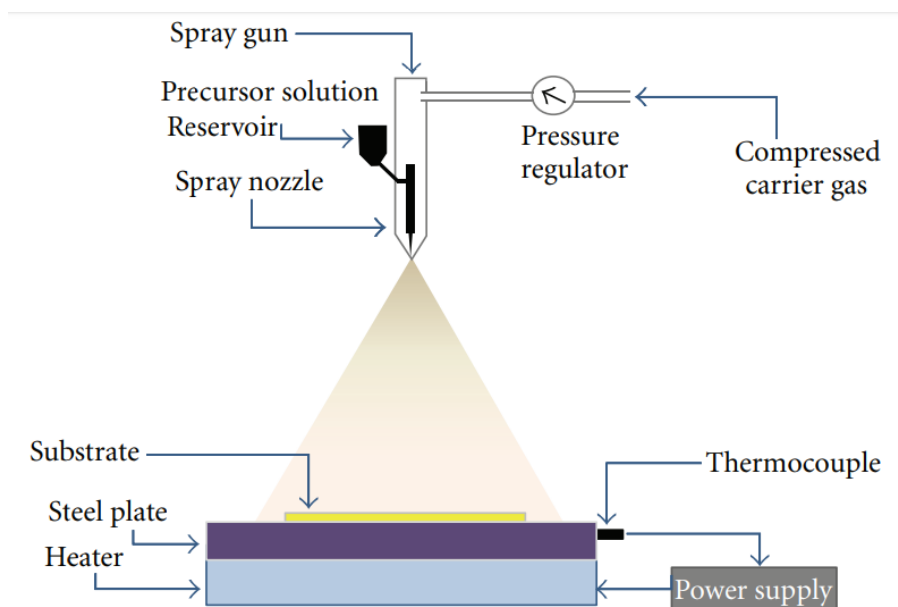


Figure 1. 4 Schematic representation of a spray pyrolysis system [11].

Spray pyrolysis process consists of many steps taking place either in consecutively or simultaneously. These steps are listed as aerosol generation and transport, solvent evaporation, droplet impact and precursor decomposition. As one of the main parameters affecting these steps, temperature has the strongest effect during aerosol generation. However, the effect on the other steps mentioned above is undeniably important. It directly affects thin film morphology and properties. Film morphology shows a transition from cracks to porous structure as temperature increases. In literature, most of the studies indicate that the most important parameter is the decomposition temperature [10].

By controlling the change in coating temperature, properties of the thin films can be altered. In the study of Margoni et al., ammonium meta vanadate was used to prepare precursor solution to obtain vanadium pentoxide thin films. As the deposition temperature increased from 300 °C to 375 °C, crystallite size of vanadium pentoxide thin films was found to increase. This change in the deposition temperatures influenced average visible transmittance and the wavelength at the maximum transmittance of the thin films. At the highest deposition temperature, vanadium pentoxide films showed the highest transmittance which may be useful in thermochromic and electrochromic devices. Also the conductivity and mobility of the deposited film at a deposition temperature of 375 °C was found to be highest temperature among other thin films deposited at 300 °C. This study simply showed the importance of deposition temperature on the optical, electrical and structural properties of thin films [12].

Huang et al. investigated V₂O₅ deposition temperatures of 250 °C and 400°C. Films deposited at 250 °C was found to be amorphous while those deposited at 400 °C showed orthorhombic crystal structure. This study clearly showed that the deposition temperature have a remarkable influence on the crystallinity of the deposited thin films [13].

1.1.2.3.2 Thin Film Deposition Models by Spray Pyrolysis

Although there are many processes occurring either consecutively or simultaneously during film formation, these can be modelled as step by step up to date. These models cover atomization, droplet transport and evaporation, decomposition of solution on the substrate and drying steps. Good understanding of these mechanisms directly affects the properties and quality of the films to be produced. The mechanism of spray pyrolysis can be basically grouped as precursor solution atomization, aerosol transportation and decomposition of the solution on the substrate basically [14].

1.1.2.3.2.1 Atomization of Precursor Solution

The working principle of the device used for atomization should be understood first to comprehend the atomization of liquids. Type of atomization devices, atomizer parameters, solution properties and process conditions are interlinked to each other. Atomizers differ in terms of the obtained droplet size, atomization rate and the initial velocity of the droplets. Air blast, ultrasonic and electrostatic atomizers are mainly used in spray coating method [15]. Typical droplet diameters and droplet velocities for the different atomizers are provided in Table 1. 1.

Table 1. 1 Characteristics of atomizers.

Atomizer	Droplet diameter (μm)	Droplet velocity (m/s)
Air Blast	5-50	5-20
Ultrasonic	1-100	0.2-0.4
Electrostatic	5-70	1-4

Air-blast atomizers use high-speed air to produce an aerosol from a precursor solution. Increasing air pressure decreases the average diameter of the produced droplets. Conversely, increasing fluid pressure results in an increase in the average droplet diameter. Increasing the distance between the spray nozzle and the surface to be coated reduces the heating effect, which results in a reduced deposition rate. This increases

covering area. The flow rate is found to have a very small effect on the spray properties.

With the ultrasonic atomizer, the precursor solution is ultrasonically stimulated using piezoelectric crystals to produce very fine droplets. Droplet size in the micron or submicron range can be controlled by the crystalline oscillation frequency. An advantage of this technique is that the gas ratio is free of aerosol ratio. Moreover, ultrasonic nozzles necessitate relatively small amounts of energy.

Electrostatic atomizers utilize electric field to form droplets of precursor solution. There are basically two types of spray modes based on this mechanism: cone-jet and multi-jet mode. Differences between these two modes are illustrated in Figure 1. 5. For the cone jet mode nozzle, the convex shape of the liquid surface is disrupted by an electric field to form a Taylor cone enlarged by a small diameter permanent jet. In multi-jet mode, the liquid is multiplied by several different jets of small diameter at the end of the tube nozzle [16].

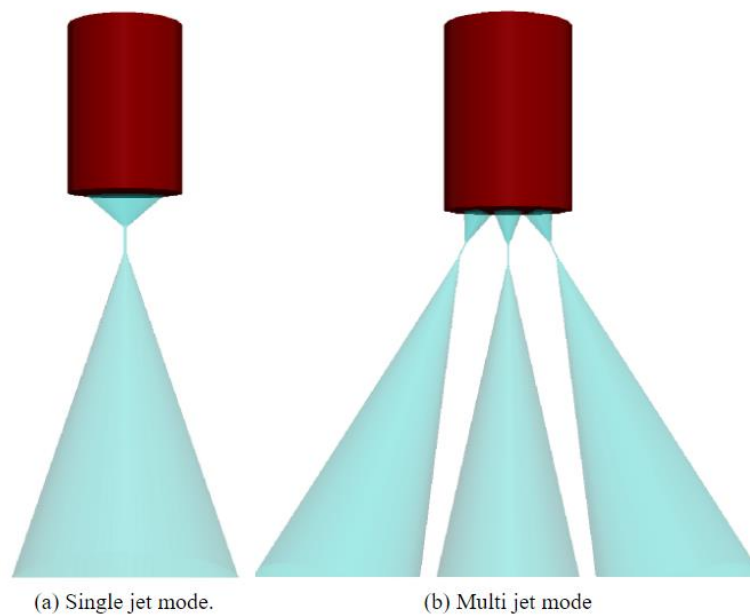


Figure 1. 5 Illustration of cone-jet and multi-jet modes [17].

1.1.2.3.2.2 Aerosol Transport

After the droplet leaves the atomizer, it moves along the perimeter at an initial rate determined by the atomizer. In aerosol form, the droplets are carried with the aim of as many droplets as possible to reach the surface. As the droplets move, they undergo physical and chemical changes [14].

As the droplet passes through the ambient, there are four forces acting simultaneously on it to determine its path. These forces are listed as gravitational, electrical, thermophoretic, and the Stokes force.

The force of gravity is the force that pulls the droplet downwards. The magnitude of the force depends on the mass of the moving droplets, a function of its volume and density.

The electrical force can be applied to spray pyrolysis systems comprising an additional electrical source that regulates the droplet trajectory. The ultrasonic atomizers are electrically driven so that an electric generator vibrates at ultrasonic frequencies. Smaller droplet sizes can be obtained by increasing the frequency. Strong electric force is used by electrostatic atomizers at the liquid-gas interface to form charged gas droplets.

The friction between the droplet and the air molecules causes drag due to the air resistance in the environment. This is called as Stokes force and derived from particle velocity and size.

The retardant force, which greatly reduces the velocity of the droplets when approaching the heated substrate, is called thermophoretic force. Air temperature increases perpendicularly due to the forced convection cooling effect of the air flow when it is close to the heated substrate. Since the thermophoretic force is dependent on the thermal gradient in the transport medium, movement of the droplets are not highly affected by this force. However, when using air-blast and ultrasonic atomizers, it may keep droplets away from the heated substrate. Moreover, film can deposit from

the vapor due to hot surface and some droplets transform to powder upon contact with the substrate. This mechanism is schematically explained in Figure 1. 6.

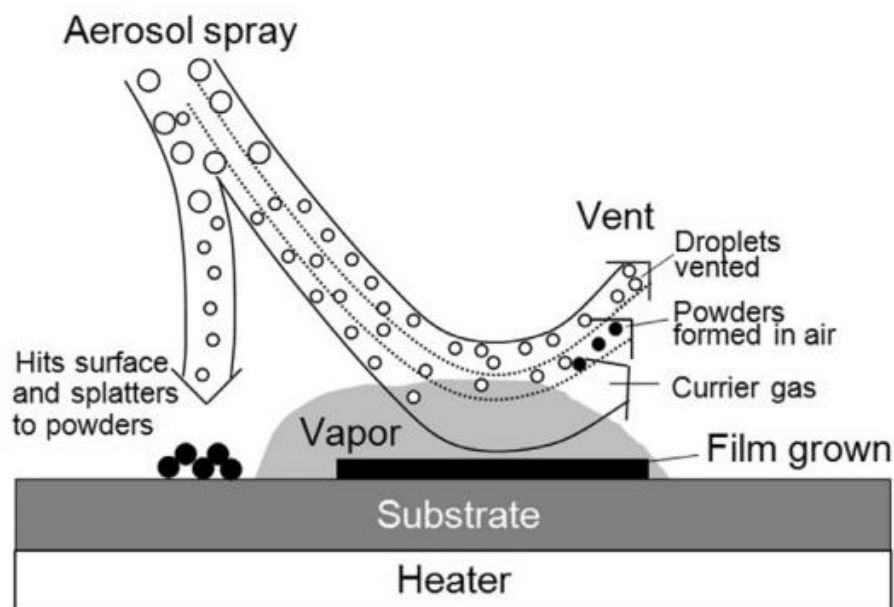


Figure 1. 6 Schematic of aerosol transport mechanism [17].

1.1.2.3.2.3 Decomposition of Precursor

When droplets reach the heated substrate surface, many processes like solvent evaporation, spreading of droplets and decomposition of salt occur simultaneously. Depending on these processes, precursor solution undergoes some changes as long as it continues to move on the heated substrate. These changes are shown in Figure 1. 7. A, B, C and D represents four potentials of moving droplets through the heated ambient during spray pyrolysis. Only process C is defined as chemical vapor deposition (CVD) like decomposition mechanism [15].

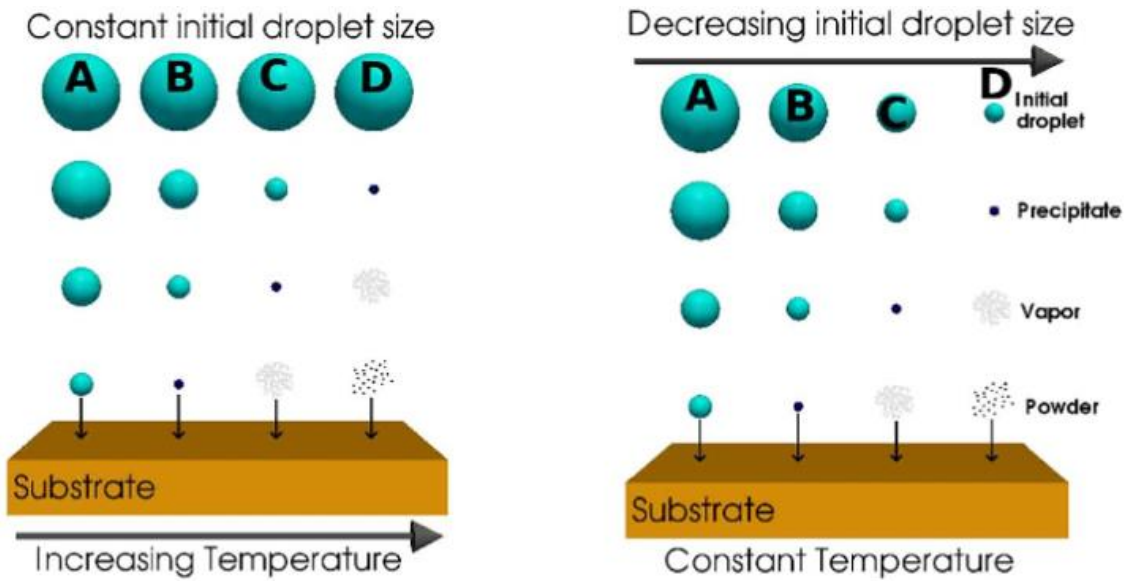


Figure 1. 7 Decomposition processes with increasing temperature [15].

In the case of process A, when large droplets come in touch with the heated substrate surface and the temperature is not high enough to completely evaporate the solution, they hit the substrate and decompose. During contact, droplets evaporate completely and leave dry precipitates. The substrate temperature decreases slightly at the point of impact due to the heat requirement for evaporation and this adversely affects the reaction kinetics. This process leads to poor adhesion.

During Process B, some solvent evaporates while average size droplets form. When decomposition occurs on the substrate surface, dry precipitates in amorphous structure form. Some of them evaporate and accumulate in between the particles. Nevertheless, the possibility of moderate adhesion occurs in this type of process.

Process C is known as the classical CVD reaction mechanism. Under the influence of environmental conditions, some droplets evaporate and become particulates before they strike the heated surface. As the particles approach the substrate surface, they pass to the vapor phase and undergo a series of heterogeneous reactions. This creates highly dense and highly adherent thin films.

Process D tries to clarify the powder formation mechanism. In case the temperature is not high enough or the particles are formed first, precipitates vaporize and chemical reactions occur immediately. These reactions in vapor phase are homogeneous and one obtain crystallites in the form of condensed powders.

1.2. Characterizations of V_2O_5 Thin Films

1.2.1. Structure and Morphology

In the vanadium oxide system, V_2O_5 is the highest oxidation compound with an orthorhombic layered crystal structure as shown in Figure 1. 8 [18]. This layer structure is in the $Pmmn$ space group and looks like a square pyramid with zigzag ribbons. Pyramidal VO_5 units builds double chains in b -direction by sharing edges and these chains are connected by their corners. Layers which are linked by weak van der Waals bonds to each other are arranged in the c -direction. Resulting shape consist of distorted octahedral VO_6 units with a 3 main $V-O$ distances. $V-O$ (1) = 1.58 Å represents vanadyl oxygen on the c -direction. In the basal plane, $V-O$ (2) = 1.77-2.02 Å indicates bridging between oxygens and weak bonds between the layers are equals to 2.79 Å [19]. Crystal structure parameters are listed in Table 1. 2. V_2O_5 is the semiconductor with a band gap of 2.24 eV [20].

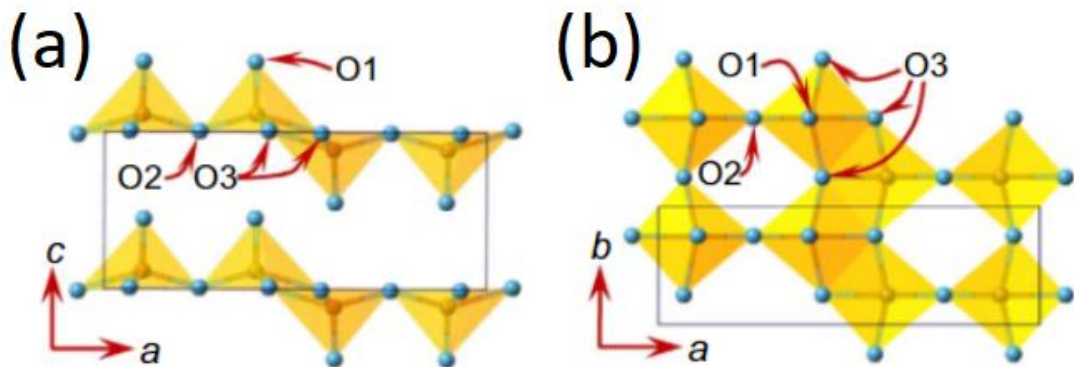


Figure 1. 8 Crystal structure of orthorhombic V_2O_5 . Views from (a) ac plane and (b) ab plane. V atoms are shown in yellow and O atoms are in blue [21].

Table 1. 2 Atomic positions in orthorhombic V_2O_5 (space group $Pmmn$).

Atom	Wyckoff Position	Parameters		
		x	y	z
V	4f	0.10118	0.25	-0.1083
O _{van}	4f	0.10430	0.25	-0.469
O _{br}	2a	0.25	0.25	0.001
O _{ch}	4f	-0.0689	0.25	0.003

Representative XRD spectra of V_2O_5 thin films is given in Figure 1. 9. Samples deposited by e-beam evaporation method at low substrate temperatures are amorphous. On the other hand, crystallized structures can be obtained by increasing deposition temperature or increasing oxygen partial pressure [22]. Typical peaks are observed around 2θ values of 20.26° and 41.4° correspond to the (001) and (002) planes of orthorhombic structure. Highly crystallized films show preferential c-axis orientation due to the dominant (001) reflection [23]. At higher substrate temperatures, redeployment process of V-O-V chains clarifies increasing in the intensity of (101) reflection. Regardless of the coating method, this behavior is typical for V_2O_5 thin films deposited by several different methods: RF sputtered using Vanadium target and Ar [24], spin-coated and annealed [25], pulsed-laser deposited on different substrates[26], using plasma enhanced CVD technique[27]. Highly ordered V_2O_5 thin films in (001) reflection were obtained through the oxidation of vanadium layer by Guimond et al. [28]. Moreover, V_2O_5 thin films deposited by sol-gel derived techniques, showed complicated behavior due to their water content. In the study of Cezar et al.[29], thin films were obtained from a precursor solution containing V_2O_5 and hydrogen peroxide (H_2O_2). XRD pattern of the films showed two different behavior . Films annealed at $150^\circ C$ were in crystalline form and showed dominant (110) reflection. However, when films were annealed at $300^\circ C$, this dominant reflection was faded and (00l) reflections started to dominate the XRD pattern. It is

also reported that spin-coated V_2O_5 thin films are amorphous when annealed below $350\text{ }^\circ\text{C}$ [30].

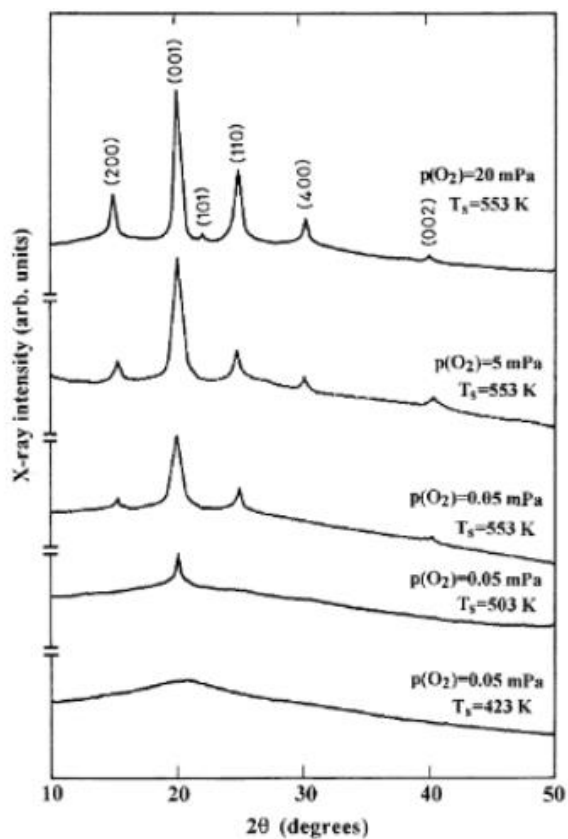


Figure 1. 9 X-Ray diffraction pattern of V_2O_5 films as a function of the oxygen partial pressure in the chamber deposition [31].

Morphology and topography of thin films on glass substrates by SEM and AFM as a function of temperature investigated by Kumar et. al.[32]. AFM images of the thermally evaporated V_2O_5 thin films are provided in Figure 1. 10 .Grain size and surface roughness of the thin were found to increase with the surface temperature. Although films deposited at $300\text{ }^\circ\text{C}$ have high crystallinity, low transmittance values were obtained with increased deposition temperature. this was attributed to increased scattering in correlation to the surface roughness of thin films. This study provided evidence on the effect of substrate temperature during deposition.

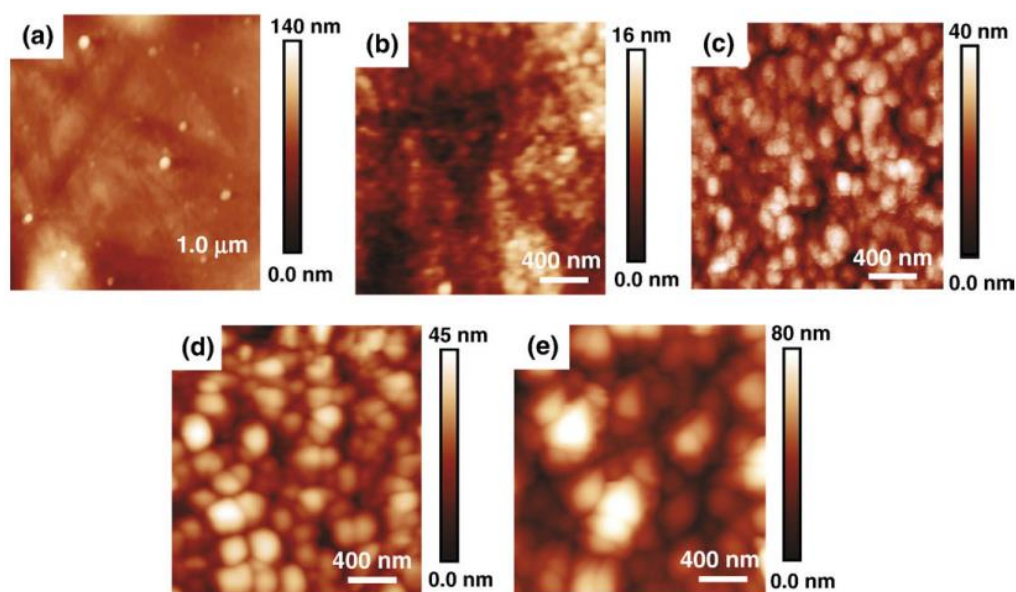


Figure 1.10 AFM images of the V_2O_5 films at (a) room temperature, (b) room temperature with a smaller scan area, (c) post-annealed film deposited at room temperature, (d) 300 °C and (e) 500 °C [32].

In the Senapati and Panda's study, spin coated V_2O_5 thin films were used to investigate the effect of solution aging on the mechanical, optical and electrical properties. SEM images provided in Figure 1.11 show that surface morphology changes from featureless one to the one that contains homogeneous ribbon-like nanostructures with the aging of solution. Optical band gap of the films was found to decrease from 2.66 eV to 2.36 eV, while the microstrain was found to decrease from 4.93×10^{-3} to 2.62×10^{-3} for a fresh solution and 192 h aged solution, respectively. This change was attributed to the loss of water [33].

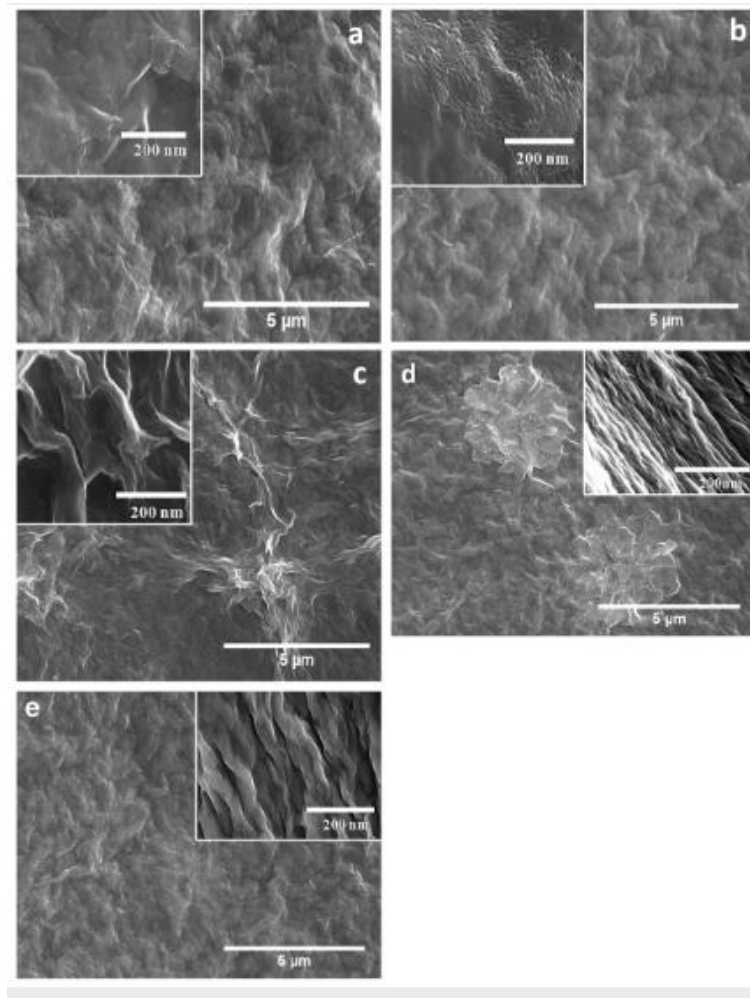


Figure 1.11 SEM images of V_2O_5 thin films prepared from (a) freshly prepared, (b) 48 h, (c) 96 h, (d) 144 h and (e) 192 h aged sol [12].

In another study, the differences in structural properties of pure and fluorine (F) doped vanadium oxide thin films were investigated. Pure vanadium oxide films were deposited by spray pyrolysis using 0.1 M ammonium metavanadate (NH_4VO_3) and F-doped films were obtained by adding 5, 10, 15 and 20 wt.% ammonium fluoride into the precursor solution. Thin films deposited onto the glass substrates were annealed at 400 °C. XRD results indicated the presence of β - V_2O_5 , V_2O_5 and V_3O_7 phases. Long flake like structures were observed on the surface of V_2O_5 films, while F-doped V_2O_5 films had rod like structures with spheroidal grains [12].

1.2.2. Optical Properties

The optical properties of thin films are usually investigated in three different ways; which are measurement of absorption to determine optical band gap, spectral window of electrochromic films and dispersion parameters. Optical absorption coefficient (α) is calculated using following equation:

$$T = \frac{[(1 - R)^2 \exp(-\alpha d)]}{[1 - R^2 \exp(-2\alpha d)]}$$

where T and R are the spectral transmittance and reflectance and d is the film thickness, respectively. The interference effect is negligible due to internal reflection at normal incidence for higher optical density ($\alpha d > 1$) that reduce above equation to [34]:

$$T \approx \exp(-\alpha d)$$

and the optical absorption coefficient becomes [35]:

$$\alpha = -\left(\frac{1}{d}\right) \ln(T)$$

The optical bandgap E_g^{opt} of a semiconductor is calculated using the interband absorption theory:

$$\alpha h\nu_i = A (h\nu_i - E_g^{\text{opt}})^n$$

,where ν_i is the incident photon energy, A is a probability parameter and n is the transition coefficient with $n = 2$ for indirect transition and $n = 3/2$ for direct bandgap for V_2O_5 [36].

Optical transmittance of V_2O_5 is well characterized in several studies. Transmittance spectra of the films coated using different substrate temperatures as 300K, 423 K and 500 K is provided in Figure 1. 12. There is a sharp fundamental absorption edge around 500 nm for all films. For films formed at higher temperatures, broad absorption band is observed around 1000 nm and films coated at low temperatures show higher

transmittance. Transmittance of the films decreases in parallel with the increase in the substrate temperature [37].

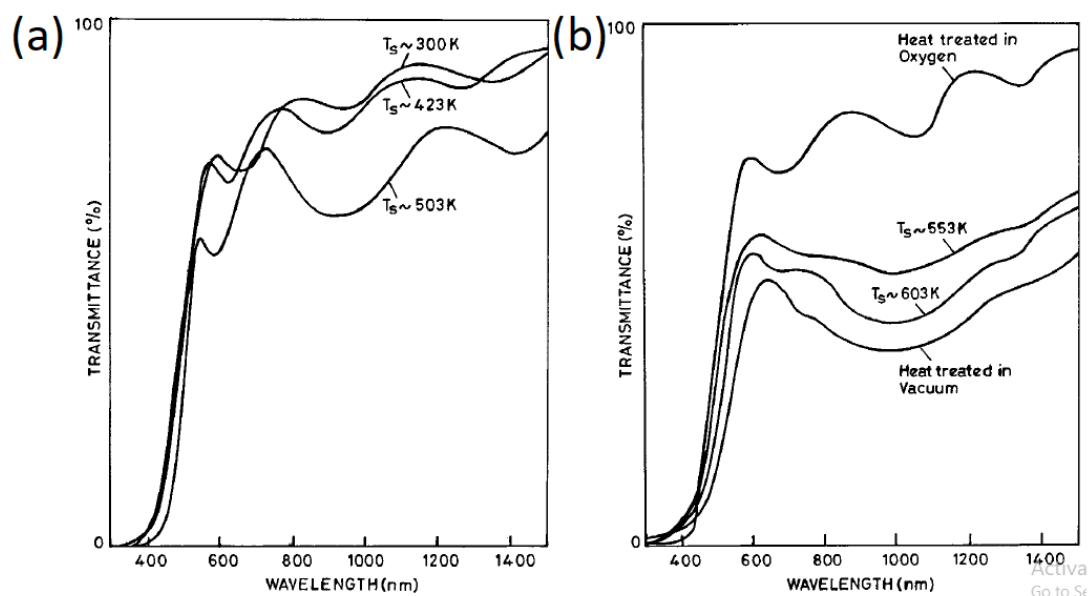


Figure 1.12 Optical transmittance spectra of V_2O_5 films formed at substrate temperature (a) smaller than 503 K and (b) larger than 503 K [37].

According to the Ramana and Hussain [38], optical absorption spectra, electron paramagnetic resonance (EPR) spectra and electrical conductivity have some characteristics like polarons arising from oxygen vacancies. They reported excess electrons in empty 3d orbitals of vanadium atoms. V^{5+}/V^{4+} pairs are closed to oxygen vacancies and this results in an absorption in the infrared spectrum. There is a sharp increase in the optical transmittance of V_2O_5 thin films deposited by e-beam evaporation within the spectral range of 550–600 nm. With the increase in oxygen partial pressure, absorption edge of the thin films are found to blue shift.

Lourenço et al. investigated the effect of oxygen flow rate (OFR) on optical characteristics of V_2O_5 thin films deposited using r.f. sputtering. When films are deposited at low OFR (1 sccm), films with the highest bandgap of 2.56 eV was obtained [39]. For higher OFR values, optical bandgaps were reported to lie in the

range of 2.41-2.45 eV. Similar studies in literature for r.f. sputtered V₂O₅ thin films reported E_g values ranging from 2.15 to 2.40 eV. [40]

Work function of V₂O₅ thin films deposited by atomic layer deposition (ALD) method is investigated by Song et al. Thin films were amorphous initially and then, to obtain crystallized thin films, post deposition heat treatment was applied at 500 °C for 1 hour under ambient conditions. Ultraviolet photoelectron spectroscopy (UPS) analysis showed a valance band gap edge (E_v) of 2.45 eV which is below the fermi level (E_F) with an E_g of 2.63 eV for annealed V₂O₅ thin films. [41]

Irani et al. investigated structural and optical properties of V₂O₅ thin films deposited using spray pyrolysis [42]. Substrate temperature was found to have prime importance in obtaining films with (001) orientation with the orthorhombic structure. Crystalline size was found to increase with the substrate temperature reaching to a maximum at 450 °C. Beyond this temperature, crystallite size was found to decrease. Highest optical transmittance was observed at a substrate temperature of 550 °C with a shift of absorption edge from 2.5 to 2.8 eV. This was attributed to the formation of chemical bonds between substrate and V₂O₅ thin film.

1.2.3. Electrical Properties

As a result of the oxygen non-stoichiometry related with oxygen vacancies V₂O_{5-δ}, V₂O₅ is classified as n-type semiconductor. To investigate electrical conductivity, DC four-point probe technique and AC impedance spectroscopy are used based on deposition and heat treatment parameters [43].

The conductivity depends on the temperature can be evaluated in a wide temperature range in accordance with the Arrhenius rule. Transition-metal ion shows various valance state like V⁺⁴ and V⁺⁵ for V₂O₅ as a common circumstance of the attitude of semiconductors. Therefore, bouncing of electrons occurs between these two states. The number of charge carriers is estimated using following formula:

$$N = CA^{-3}$$

, where C is the ratio of the concentration of low valence ion to total transition-to-metal ion concentration ($C = V^{+4} / (V^{+4} + V^{+5})$) and A is the average distance for electron hopping. A very low electron mobility within the range of 10^{-7} and 10^{-2} $\text{cm}^2/\text{V}\cdot\text{s}$ was obtained upon taking C as 0.02 nearly and A as 0.384 nm [44].

Some researchers also claim that thermally activated hopping occurs in electronic states causes electron transport for amorphous films deposited by flash evaporation [22] and PVD techniques [45]. Electrical conductivity (σ) which follows the Arrhenius law and the activation energy which depends on the substrate temperature and post heat treatment parameters of flash evaporated amorphous V_2O_5 thin films are provided in Figure 1. 13 . Even if heat treated, thin films deposited at room temperature showed lower σ values compared to other films deposited at higher temperatures. The conductivities of as-deposited films were found to be lower than those annealed under argon, which is lower than those annealed under oxygen. Activation energy of as-deposited films at room temperature was 0.43 eV. On the other hand, activation energy of heat treated films under oxygen environment was 0.15 eV. Moreover, there was a sharp decrease in the resistivity of films from $\rho = 5 \times 10^4 \Omega \text{ cm}$ for as-deposited condition to $\rho = 0.62 \Omega \text{ cm}$ for annealed condition. One can expect that C was directly affected by the substrate and annealing temperatures because of the removal of oxygen during deposition. The increase in the conductivity was mainly considered as a result of the change in crystal structure from amorphous state to polycrystalline and the lack of oxygen in the films obtained at high temperatures with a small oxygen/vanadium ratio. Luo et al. investigated the effect of substrate temperature on the electrical properties of thin films. These films were deposited using DC sputtering onto different substrates as potassium bromide (KBr) and glass [46]. Electrical measurements using four-probe method showed that there is an exponential decrease in the sheet resistance of films from 46 to 32 $\text{k}\Omega/\square$ upon increasing the substrate temperature from 230 to 320 $^\circ\text{C}$.

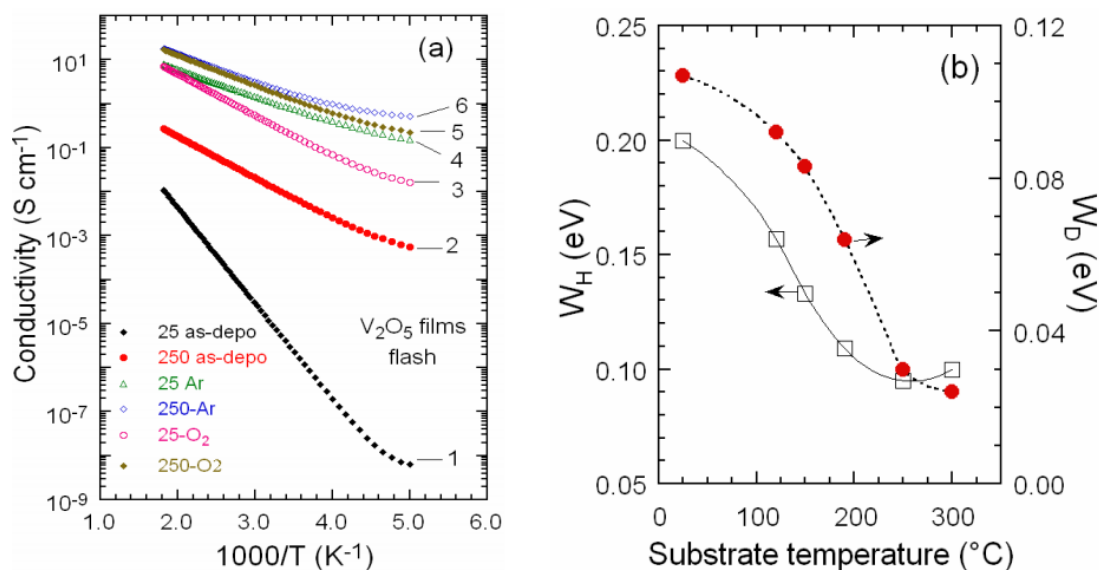


Figure 1.13 (a) Plots of σT vs. $1/T$ for flash-evaporated V_2O_5 films obtained in various conditions. (1) as-deposited at $T_s = 25^\circ\text{C}$, (2) as-deposited at $T_s = 250^\circ\text{C}$, (3) grown at $T_s = 25^\circ\text{C}$ and annealed in O_2 , (4) grown at $T_s = 25^\circ\text{C}$ and annealed in Ar , (5) grown at $T_s = 250^\circ\text{C}$ and annealed in O_2 and (6) grown at $T_s = 250^\circ\text{C}$ and annealed in Ar . The annealing treatment was carried out at 300°C for 48 h. (b) Plots of σRT and Wh vs. T_s [47].

Santos showed that thermally evaporated and heat treated at 500°C crystalline V_2O_5 thin films display thermoelectric characteristics. A maximum Seebeck coefficient of $-218 \mu\text{V K}^{-1}$ was reported with an electrical conductivity of 0.055 S cm^{-1} [35].

Rosaiah et al. investigated the effect of substrate temperature for V_2O_5 thin films deposited through e-beam evaporation onto ITO-coated Kapton substrates. Results showed that the conductivity of films increases from 2×10^{-6} to $3 \times 10^{-2} \text{ S cm}^{-1}$ with the substrate temperature increasing from 30 to 300°C [34].

Wang et. al. showed that thick polycrystalline V_2O_5 films can also perform as a hole-extraction layer for photovoltaic devices [48].

1.3. Applications of V₂O₅ Thin Films

List of demonstrated applications of V₂O₅ thin films include but not limited to lithium-ion batteries [49][38], optical switching memories [50], thin-film micro batteries [50][51][52], antireflection coatings [53], catalysis [54], electrochromic devices[55] .

1.3.1. Supercapacitors

Supercapacitors, basically electrochemical capacitors (ECs), consist of two subgroups which are electrochemical double layer capacitors (EDLCs) and pseudocapacitors. Although EDLCs display non-faradaic charge characteristics, pseudocapacitors are mainly based on faradaic electrochemical reactions. Due to wide range oxidation states, high capacitance and pseudocapacitive characteristics, nanostructured V₂O₅ has attracted significant attention as an electrode material. However, the number of studies that utilizes V₂O₅ thin films in the supercapacitors is quite low [56][57][58] .

Sandhya et al., utilized DC magnetron sputtered V₂O₅ thin films on Ni substrates with a preferable orientation along (001) direction as supercapacitor electrodes. A specific capacitance of 238 F g⁻¹ was reported at a current density of 1 mA cm⁻² . Films had a grain size and roughness 32 nm and 14 nm, respectively [58].

In another study by Prakesh et. al., V₂O₅ thin films on Ni substrates were obtained by thermal evaporation at 250 °C using molybdenum (Mo) as a dopant at different concentrations. A maximum specific capacitance of 175 F g⁻¹ was achieved from films with a Mo doping of 4 at.% [56].

1.3.2. Gas Sensors

V₂O₅ thin films have been utilized widely as a gas sensor due to their unique catalytic characteristics. The V⁵⁺ ions with d⁰ electronic configuration form active sites allowing catalytic reactions to occur and the gas molecules to easily attach to the surface [59][60]. V₂O₅ thin films are typically incorporated into sensors used for volatile organic compounds (VOCs) such as benzene, acetone, toluene, methanol which are very dangerous for human health and the environment

[61][40][62][48][63]. It is reported that the highest sensing response was observed for ethanol, V_2O_5 thin films obtained by spray coating method at a substrate temperature 300 °C substrate temperature [60].

Sensing behavior of polycrystalline V_2O_5 thin films deposited by spray pyrolysis method was investigated by Vijayakumar et al. [64]. It is revealed that these films are very sensitive to VOCs in particular to xylene. Response of V_2O_5 films at deposited at a substrate temperature of 300 °C towards various VOCs is provided in Figure 1. 14.

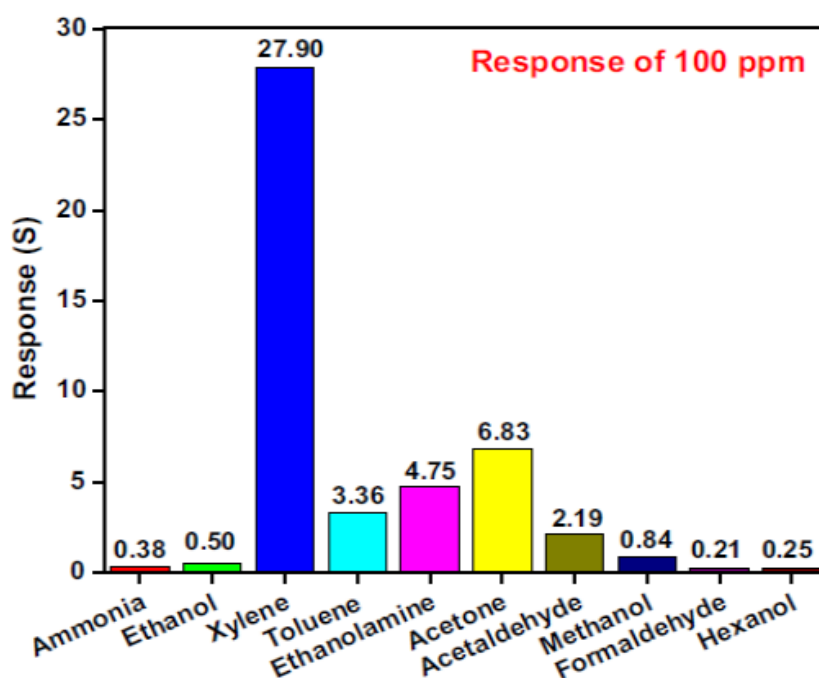


Figure 1. 14 Response of V_2O_5 films prepared by spray pyrolysis at a substrate temperature of 300 °C for different VOCs vapors at a concentration of 100 ppm [64].

In addition to the VOCs, solid state sensor with nanocrystalline V_2O_5 were fabricated for the detection of ammonia [59].

V_2O_5 thin films with thicknesses between 200-600 nm deposited using RF sputtering at 290 °C are also used as gas sensors. Highly promising response against methane,

propane (50-3000 ppm) and hydrogen (5-300ppm) was obtained [65]. Moreover, DC sputtered V_2O_5 films also showed promising response to sense the presence of 2-propanol under ambient conditions [66].

1.3.3. Electrochromic Devices

Electrochromic devices (ECDs) basically consist of three main layers that are electrochromic layer, electrolyte and ion storage layer. A schematic design of ECD is given Figure 1. 15. Electrochromic and storage layers are deposited onto transparent conductive oxide (TCO) coated glass substrates. The working principle of electrochromic devices depends on the change of optical properties in different color ranges. In the ECD system, V_2O_5 thin films are used as counter electrode [67][68][69]. Electrochemical redox reactions result in a change in the optical properties of V_2O_5 thin films. These reactions utilized that balance charge transfer at the electrochromic working electrode.

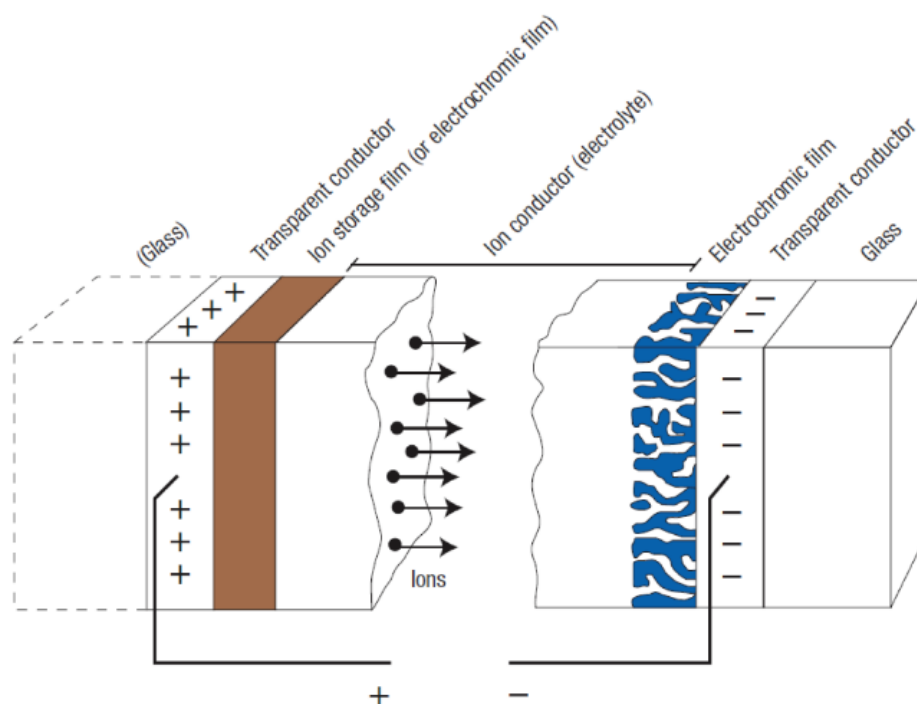
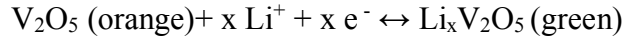


Figure 1. 15 Electrochromic device design, showing the movement of ions under an externally applied electric field [70]

The double injections of electrons and ions explain the typical electrochromic reaction of V_2O_5 which is as follows:



,where ion molar fraction is indicated as x and inserted in the host lattice. Moreover, the transmittance variance (ΔT) is described by [71]:

$$\Delta T (\%) = T_b - T_c$$

Transmittances (%) of bleached and colored state are indicated as T_b and T_c . One of the most important parameters in determining the properties of EC devices and materials is the coloring efficiency (CE). It is simply the change in optical density (OD) per unit of charge (Q). The high CE value of EC films ensures that a large optical modulation range can be achieved with a relatively small insertion or subtraction charges [72]. It is calculated from following equation:

$$CE = \Delta OD / (q / A) = \log (T_b / T_c) / (q / A)$$

,where q is defined as inserted charge capacity. Accordingly, color efficiency (η) is described as:

$$\eta = \Delta OD / q$$

Sarminio et al. claimed that the EC properties are directly related to the changes in stress for polycrystalline thin films. They showed that as the Li concentration in the films changes, tensile stress changes and reaches a maximum in the δ -Li V_2O_5 phase [73]. Electrochemically deposited V_2O_5 thin films on ITO-coated glass substrates were used in EC devices. After testing the device at least 8×10^4 times, the response time of the electrochromic films was reported to be between 2 and 20 sec. [35]. To enhance the EC response, the solution formed by dissolving V_2O_5 powders in benzyl alcohol and iso-butanol mixture is deposited on ITO coated glass substrates by spin coating.

Following a heat treatment is applied at 300 °C , polycrystalline V₂O₅ thin films with very high reversibility was obtained [74].

1.3.4. Solar Cells

V₂O₅, as a cost-effective material with excellent thermal and chemical stability, has received significant interest from researchers for solar cell applications. Recent literature have extensively focused on this transition metal oxides because of their favorable electronic properties, low optical absorption in the visible spectrum, and high level of technological compatibility with organic electronics.

Zhan et al. used V₂O₅ thin films as hole-extract ion layer. The effects of the morphology and the thickness of the V₂O₅ interlayer on the performance of organic solar cells (OSCs) are investigated. An efficiency that is 3 times better than the control device fabricated with bare ITO was obtained using V₂O₅ interlayer with optimized thickness.

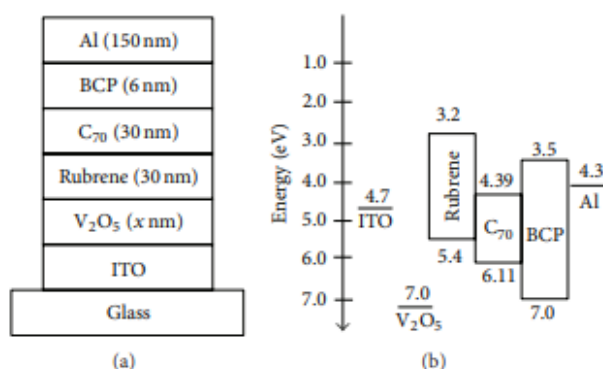


Figure 1. 16 (a) Device structure of rubrene/C₇₀-based OSCs and (b) respective energy band gap diagram [75].

Device structure and energy band diagram are given in Figure 1. 16. Due to high work function, thermally evaporated ultrathin films of V₂O₅ have a more favorable energy level alignment for hole extraction compared to bare ITO. Moreover, current density – voltage (J-V) characteristics of the device with only ITO and 3 nm thick V₂O₅ layer under 100 mW/cm² illumination is provided in Figure 1. 17. In the absence of V₂O₅ interlayer, device showed a power conversion efficiency (PCE) of 0.42% with a low

fill factor (FF) of 36.2%. The short circuit current density (J_{SC}) and open circuit voltage (V_{OC}) are 2.3 mA/cm² and 0.51 V, respectively. Through the insertion of a 3 nm V₂O₅ interlayer between the donor layer and the anode, the device showed J_{SC} , V_{OC} and FF values of 4.58 mA/cm², 0.88 V and 43.3%, respectively. A significant improvement in PCEs to 1.74% [70].

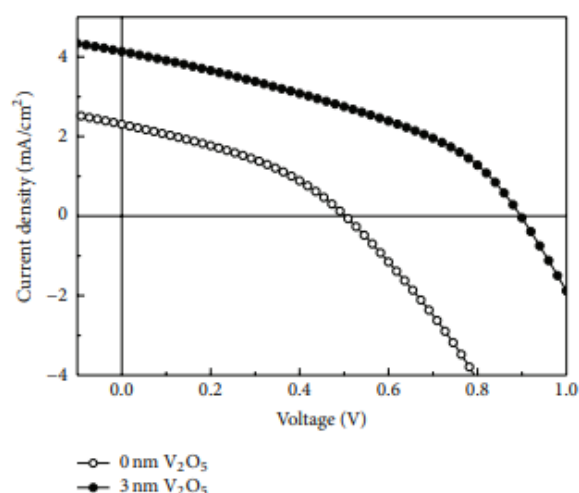


Figure 1. 17 The J-V characteristics of OSC devices with and without V₂O₅ hole extraction layer [75].

Due to the favorable electronic properties, V₂O₅ interlayer effectively extracts holes and suppresses the contact resistance. Because of the thickness dependent electrical conductivity and the optical transmittance of V₂O₅ layers, the performance of OSCs changes with the thickness of V₂O₅ layer. V₂O₅ interlayer can be used in the tandem devices [75].

V₂O₅ is a promising HTL candidate for perovskite solar cells. This is due to its high transparency to visible light and high carrier mobility with energy levels well suited for hole transport in perovskite solar cells (PSCs). Wang et al. compared V₂O₅ incorporated devices (PVO) to that of PEDOT only devices in terms of efficiency and stability. The modified devices (PVO) showed 20% higher PCE values than PEDOT only devices. The J-V characteristics obtained from PEDOT and PVO devices (A) and the device structure (B) are shown in Figure 1. 18. The J_{SC} for the PVO device was

found as 22.69 mA/cm^2 which was $\sim 20\%$ higher than that of PEDOT device ($J_{SC} = 18.86 \text{ mA/cm}^2$). The V_{OC} of the PEDOT device was found as 895.8 mV was slightly higher than that of the PVO device with 884.48 mV . The small difference in the $V_{OC} \sim 10 \text{ mV}$ between the two devices was attributed to the incorporation of V_2O_5 , which was in contact with the ITO and the associated work function difference between them. Nevertheless, the FF was similar in both devices (PEDOT device with FF of $\sim 74.08\%$ and PVO device with FF of $\sim 74.70\%$). Furthermore, the bilayer PSCs (PVO) had higher stability than PEDOT only devices; retaining 95% of their initial PCE even after 18 days of testing. The reason for the enhancement in stability was attributed to superior charge collection properties of the PVO HTL and degradation stability of the V_2O_5 nanoparticles [76].

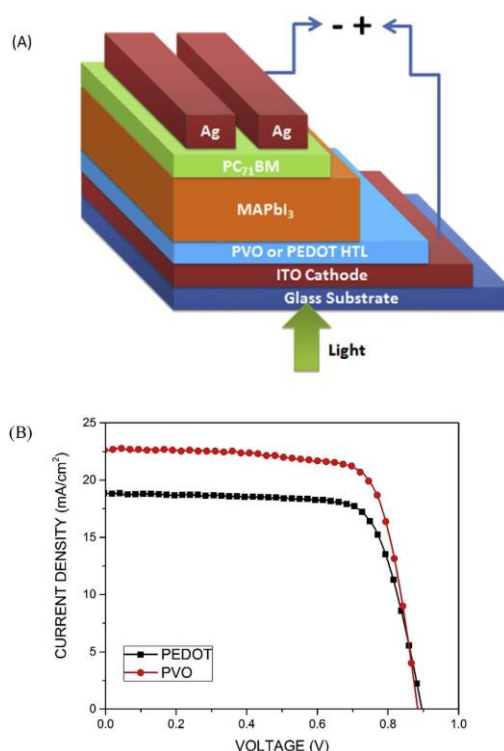


Figure 1.18 (a) The device structure diagram. (b) J-V curves of PEDOT and PVO devices[76].

Another study by Liu et. al. described a method for the production of highly stable PSCs. This highly stable device was prepared using a V_2O_5 film to modify the poly(3,4-ethylene dioxy-thiophene)-poly(styrene sulfonate) (PEDOT:PSS) hole transport

layer (HTL). The transport layers in planar PSCs can be modified using V_2O_5 and Bphen films. The J–V characteristics of the PSCs with different structures under AM 1.5G illumination is provided in Figure 1. 19. Significant effect of V_2O_5 and Bphen modified layer films on the device performance was observed. The PCE of the best-performing PSC device with V_2O_5 and Bphen modified layer was 15.49% and maintained an efficiency of more than 70% after exposure to air. The V_2O_5 modified layer was found to increase the light absorption in the perovskite active layer by reflecting the photons.

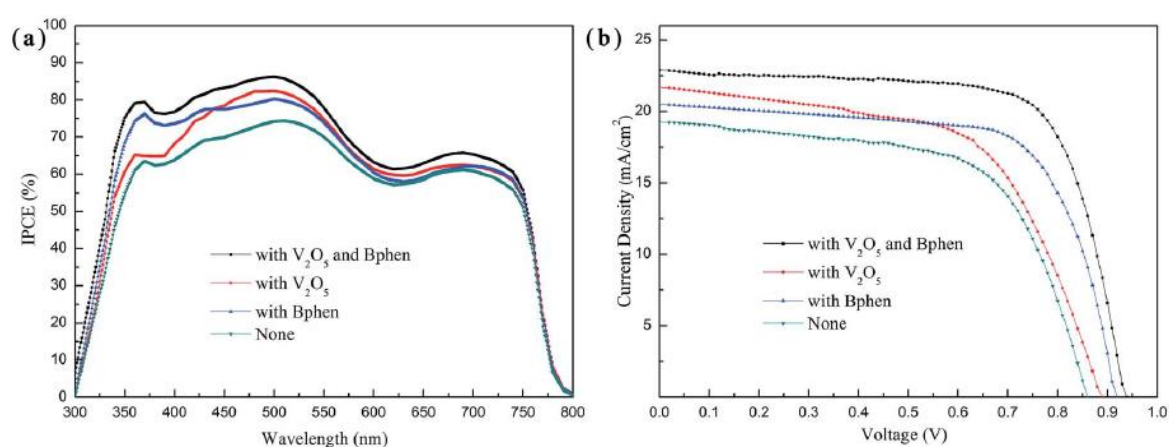


Figure 1. 19 The (a) incident photon to electron efficiency (IPCE) spectra and (b) J–V curves obtained for the PSCs with and without V_2O_5 and Bphen modified layers[77].

In addition, perovskite is extremely sensitive to water in the air. If the perovskite film between PEDOT:PSS and PCBM films comes into contact with water from the air, it gets severely damaged. Herein, the V_2O_5 and Bphen films served as protective layers effectively blocking the passage of water from the air to the perovskite film. The improvement in the stability was achieved due to the simultaneous interfacial modification of the cathode and anode. Therefore, the stability of the device with the V_2O_5 and Bphen modified layer films was significantly improved when compared to bare control devices. The stability measurement results of the PSCs in terms of PCE, V_{oc} , J_{sc} and FF are provided in Figure 1. 20 (a)-(d) respectively.

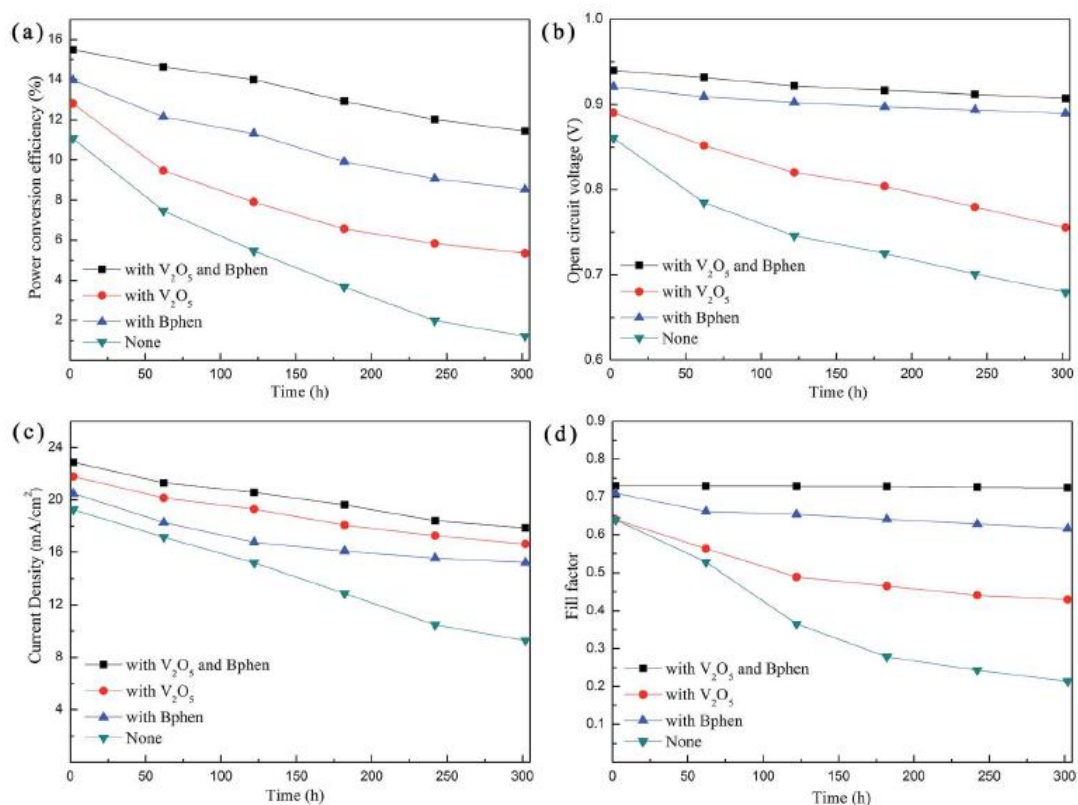


Figure 1. 20 Line charts that show the variation in the performance parameter of the four kinds PSCs with time including the (a) PCE, (b) V_{oc} , (c) J_{sc} and (d) FF [77].

This results that the perovskite layer film was protected under the Bphen modified layer film and cannot be in direct contact with air. Hence the perovskite layer film was not damaged significantly. Few of the generated electrons and holes recombine within the light absorbing layer, significantly improving the stability of the PSCs devices. When compared with the original device, the J_{sc} of the devices with the V₂O₅ film decreased slowly. This indicates that the V₂O₅ film effectively prevents the PEDOT:PSS HTL from coming into direct contact with the ITO electrode, protecting the integrity of the PSC structure and the stability of the devices [77].

1.3.5. Li Microbatteries

V₂O₅ thin films were utilized as a positive electrodes, called cathodes, in rechargeable lithium microbatteries. Devices were lithium metal anode, crystalline or amorphous V₂O₅ thin film cathode and an amorphous inorganic electrolyte [78]. The cross-section

of a thin-film lithium microbattery is provided in Figure 1. 21. The conductivity of the most prevalent solid-electrolyte thin film Lipon; $\text{Li}_{2.9}\text{PO}_{3.3}\text{N}_{0.46}$ is $2 \times 10^{-6} \text{ S cm}^{-1}$ at $25 \text{ }^\circ\text{C}$ [79]. It is deposited by RF magnetron sputtering of Li_3PO_4 in N_2 ambient. A common solid-state battery is formed by a $1 \text{ }\mu\text{m}$ thick solid electrolyte and $5 \text{ }\mu\text{m}$ thick lithium film and $1 \text{ }\mu\text{m}$ thick amorphous V_2O_5 film deposited at $25 \text{ }^\circ\text{C}$ [80][81]. Capacities of the thin film cells were interpreted using surface and thickness as $\text{mC cm}^{-2} \mu\text{m}^{-1}$ or $\mu\text{Ah cm}^{-2} \mu\text{m}^{-1}$. The theoretical specific capacity is $Q_{\text{th}} = 147.8 \mu\text{Ah cm}^{-2} \mu\text{m}^{-1}$ for a film as dense as the crystalline material when accounting the theoretical specific capacity of 440 mAhg^{-1} for $\text{Li}_x\text{V}_2\text{O}_5$ with uptake of 3 Li per formula and the density $d = 3.36 \text{ g cm}^{-3}$ of V_2O_5 .

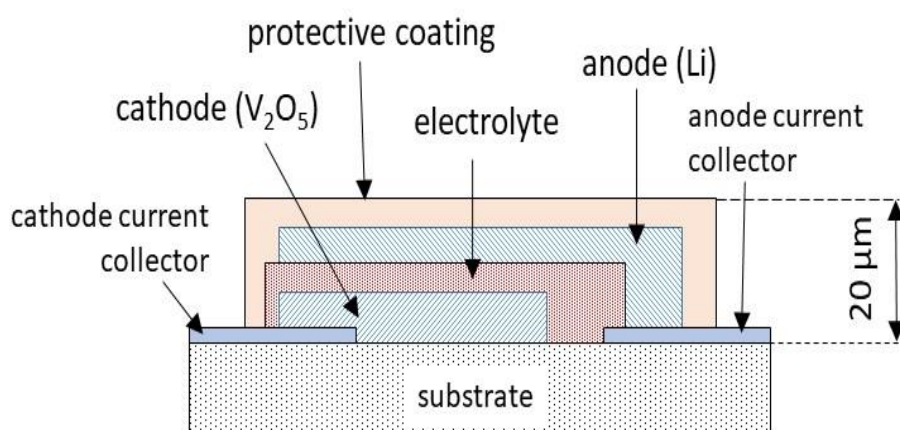


Figure 1. 21 Schematic cross-section of a thin-film lithium microbattery [47].

Bates et al. reported a capacity value of $\sim 100 \mu\text{Ah cm}^{-2} \mu\text{m}^{-1}$ at a current density of $10 \mu\text{A cm}^{-2}$ for $\text{Li}/\text{V}_2\text{O}_5$ cells cycled within a potential window of $1.5 - 3.6 \text{ V}$ [51]. PECVD, pulsed layer deposition (PLD), RF sputtering are the main methods for the deposition of vanadium oxide (VO_x) films. That type of films show high discharge capacity and are highly stable during electrochemical cycling. Although amorphous and polycrystalline V_2O_5 thin films deposited by PLD method at a substrate temperature of $200 \text{ }^\circ\text{C}$ had a discharge specific capacity of 380 mAhg^{-1} , PECVD deposited V_2O_5 films on the other hand showed the highest stability with a discharge

capacity of 408 mAhg^{-1} over 4400 cycles. It was claimed that PECVD method is more suitable for the deposition of lithium microbatteries.

CHAPTER 2

MATERIALS AND METHODS

In this chapter, materials used in the fabrication of ultrasonically spray coated and spin coated V_2O_5 thin films are listed and experimental procedures are explained. In addition, characterization techniques used to investigate the film properties are described.

2.1. Materials

The list of chemicals used in the preparation of coating solutions are given in Table 2.

1. All chemicals were used without any purification.

Table 2. 1 List of chemicals used for the preparation V_2O_5 sol.

Material	Supplier	Purity	Formula
Vanadyl acetylacetonate	Sigma Aldrich	98 %	$VO(acac)_2$
Methanol	Sigma Aldrich	≥ 99 %	CH_3OH

2.2. Experimental Procedure

2.2.1. Cleaning Procedure of Glass Substrates

FTO coated glass slides ($21 \Omega/cm^2$ - 2.00 cm x 2.00 cm) were cleaned in an ultrasonic bath for 20 min at 50 °C using acetone, Hellmanex solution, isopropanol and deionized water respectively. At the end, after the removal of remaining water on the substrates with nitrogen flow, substrates were dried on a hot plate at 100 °C.

2.2.2. Preparation of Coating Solution

The coating solution consists of two components that are vanadyl acetylacetonate as the precursor and methanol as the solvent. 0.25 M vanadyl acetylacetonate was

dissolved in 50 ml of methanol at room temperature and solution was stirred in an ultrasonic bath for 1 hour. Afterwards, the solution was aged at room temperature for 1 week.

2.2.3. Deposition of V₂O₅ Thin Films by Spin Coating

Precursor solution was coated onto glass substrates via spin coating method with Specialty Coating System G3 spin coater. The spin coating was performed at 2500 rpm with 5 sec acceleration-deceleration, and 30 sec coating. Between sequential two coating steps, films were dried on a hot plate for 15 minutes at 60 °C to obtain homogeneous and dense layers.

Several samples were obtained as 5 layers, 10 layers and 15 layers. Post heat treatment process was applied following coating process. Heat treatment temperatures were determined as 450 °C, 500 °C and 550 °C and applied for 1 hour under ambient conditions. Descriptions and designations of samples deposited by spin coating are tabulated and provided in Table 2. 2.

Table 2. 2 Designations and descriptions of the samples deposited by spin coating.

SAMPLE	ANNEALING CONDITION
SP - B	Not annealed
SP - 450	450 °C and 1 hour
SP - 500	500 °C and 1 hour
SP - 550	550 °C and 1 hour

2.2.4. Deposition of V₂O₅ Thin Films by Ultrasonic Spray Coating

2.2.4.1. Ultrasonic Spray Pyrolysis System

Sono-Tek Exacta Coating device was used to deposit V₂O₅ thin films onto heated substrates. This device consists of integrated systems listed as incorporating liquid delivery, exhaust, motion control.

In this system, 120 kHz ultrasonic nozzle type is selected as Vortex which produces stable and conical spray pattern with intermediate width. Liquid precursor solution is carried by a silicone pipe and air flow is used in ultrasonic atomization. Flow rate is automatically adjusted by means of a software of the Sono-Tek system.

The operating principle of ultrasonic nozzles is based on the transfer of high-frequency sound waves to liquid and converting them into mechanical energy. This transformation creates standing waves. At the end of the atomization process, precursor solution becomes a mist of uniform droplets. Required power to operate ultrasonic nozzle is varied between 1-8 Watts. Schematic diagram of this type of nozzle is provided in Figure 2.1.

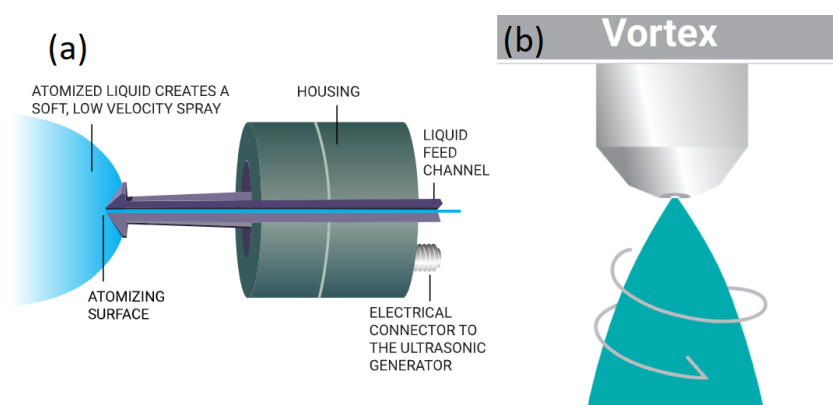


Figure 2. 1 (a) Cross-section of ultrasonic nozzle. (b) Schematic representation of Vortex type nozzle.

A hot plate is placed at the bottom of the system cabin. While the heated substrate is held in a fixed position, the nozzle performing the coating process is moved as desired in the X, Y and Z axes. Simply, the nozzle operates in a kind of coordinate system with defined positions. The direction and degree of movement are controlled either manually or automatically through the system software.

Several parameters have importance in ultrasonic spray pyrolysis. These include substrate temperature, flow rate, moving speed, distance between nozzle and substrate, amount and type of precursor solution. These parameters are tabulated and provided in Table 2. 3. These eventually determine the structural and morphological properties

of deposited thin films. Therefore, these parameters have to be comprehensively optimized.

Table 2. 3 Parameters of ultrasonic spray pyrolysis system.

USP System Parameters	Precursor Solution Parameters
Substrate Temperature (°C)	Molarity (M)
Flow Rate (ml/min)	Type of Solution Components
Air Pressure (kPA)	Viscosity (kg/s.m)
Nozzle and Substrate Distance (cm)	pH
Amount of Deposition (ml)	
Annealing Temperature (°C)	

2.2.4.2. Deposition by Sono-Tek Exacta Coat System

For use in the spray system, the precursor solution prepared previously was diluted to 0.025M by adding methanol. During spray pyrolysis, substrate temperature was set at 100 °C and distance between nozzle and substrate was 9 cm. To improve adhesion of films, flow rate is selected as minimum as possible with 0.1 ml/min. An air pressure of 3 kPa air pressure was used.

During the coating process, the ultrasonic nozzle follows a path drawn using the Path Master program. Path follows sinusoidal trajectory in X and Y direction. Spacing area between two top points was set as 2 mm. In order to obtain thin films with maximum homogeneity, an offset value of 1 mm in each cycle was used.

A post heat treatment process was applied to the films following deposition process. It is reported in literature that the thin films deposited above 450 °C are crystalline, while those deposited below this temperature are amorphous. Therefore, heat treatment temperatures were determined as 450 °C , 500 °C and 550 °C in this work. Annealing was practiced for 1 hour under ambient conditions. Descriptions and designations of samples deposited by ultrasonic spray pyrolysis method are tabulated and provided in Table 2. 4.

Table 2. 4 Designations and descriptions of the samples deposited by spray pyrolysis.

SAMPLE	ANNEALING CONDITION
USD - B	Not annealed
USD - 450	450 °C and 1 hour
USD - 500	500 °C and 1 hour
USD - 550	550 °C and 1 hour

2.2.4.3. Optimization of Spray Pyrolysis System

As studied earlier, ultrasonic spray pyrolysis method is influenced by various parameters. Molarity of the precursor solution, substrate temperature, flow rate, air pressure of the shaping gas and decomposition path should be optimized since they affect crystal structure, surface morphology and thickness of the thin films. Parameters with respective values investigated in this thesis tabulated and provided in Table 2. 5.

Table 2.5 Summary of optimized USP parameters

Parameters	Values
Molarity of Precursor Solution	0.025 M, 0.25 M
Substrate Temperature	60 °C, 80 °C, 100 °C
Flow Rate	0.1 ml/min, 0.25 ml/min, 0.5 ml/min
Air Pressure	1 kPa, 2 kPa, 3 kPa, 4 kPa.

First step in the process optimization is the determination of molarity of the precursor solution. While other parameters were kept constant, solutions with different molarity values (0.025 M and 0.25 M) were prepared. It is important to note that, no agglomeration was observed in the prepared solutions with time. When the solution concentration was 0.25 M, precursor solution blocked the tip of the cancelling the flow. In addition, the surface quality of the deposited films got adversely affected from the local precipitates. Thus, a solution concentration of 0.025M was decided to be used as a precursor in order to minimize the nozzle clogging and to maximize film homogeneity.

Following solution concentration, substrate temperature was investigated as a parameter to optimize ultrasonic spray pyrolysis method. Substrate temperature directly determines the crystallinity of the deposited thin films. In accordance with the literature, substrate temperatures of 60, 80 and 100 °C were used in this work. The effect of substrate temperature was monitored by SEM analysis and visual. Lower substrate temperatures created precipitates on the film surface, therefore, 100 °C was selected as a substrate temperature for the further studies.

Flow rate directly affects the homogeneity of the deposited films. At higher flow rates, evaporation could not be controlled and the solution was found to deposit excessively along the path. Local irregularities and fluctuations on the film thickness were observed. In the experiments, 0.1 ml/min, 0.25 ml/min and 0.5 ml/min were used and it was observed that film quality increases with the use of low flow rates. Consequently, studies continued with a solution flow rate of 0.1 ml/min.

Shaping air influences the droplet size and homogeneity. It changes size and impact of the conical decomposition through the adjustment of the pressure. Air pressures of 1 kPa, 2 kPa, 3 kPa and 4 kPa were investigated. When air pressure was low, droplets could not strike the heated substrate with sufficient force to decompose. Based on the visual inspection of the coating surfaces, further studies made use of a flow rate of 3 kPa.

Lastly, Sono-Tek Exacta Coat device is able to move in 3 different axes, fixed and variable, depending on the desired path. Separation, speed of the nozzle movement, dwell time and repetition of motion are adjustable. Different paths were investigated in this work. As an optimum path, the one can be seen in Figure 2. 2 was used in further studies with different number of repetitions. Target here was to obtain homogeneous thin films with no free space left. Available minimum separation within the nozzle motion was chosen as 2 mm with an offset of 1 mm to the fill spaces through the both x and y directions.

2.3.2. X-Ray Photoelectron Spectroscopy (XPS)

In order to find surface chemical nature of the deposited thin films, X-Ray spectroscopy (XPS) was utilized. XPS analyses were performed using a SPECS PHOIBOS hemispherical energy analyzer. A monochromatic Al-K α X-Ray excitation source (15 kV, 400 W) was used.

2.3.3. Raman Spectroscopy

Raman spectroscopy was used to confirm the formation of thin films and determine their crystal structure. Raman spectra of the films were recorded using Renishaw inVia system with a laser wavelength of 532 nm.

2.3.4. Scanning Electron Microscopy (SEM)

Scanning electron microscopy (SEM) analyses were conducted for microstructural evaluation of deposited thin films using a FEI Nova Nano FEG-SEM 430 equipped with an energy dispersive X-ray analyzer operated at 10 kV. A few nanometers thick gold layer was deposited onto the samples prior to analysis in order to reduce the charging effects .

2.3.5. Atomic Force Microscopy (AFM)

Atomic force microscopy (AFM) was used to investigate the surface morphology of the films using a Veeco MultiMode V model in tapping mode. Microstructural details and roughness of the film surface were examined at respective sampling sizes of 1 x 1 μ m and 200 x 200 nm.

2.3.6. X-Ray Fluorescence (XRF)

Thickness of deposited V₂O₅ thin films were measured by X-Ray fluorescence (XRF). XRF analysis was performed using a Fischer XDV-SDD device. An acquisition time of 20 s was used at tube voltage and current of 50 kV and 0.8 mA , respectively .

2.3.7. UV-Vis Spectrophotometry

UV-Vis light transmittance of the thin films were recorded within the wavelength range of 300 to 800 nm using PG T80+ spectrophotometer .

2.3.8. Cyclic Voltammetry

In order to understand the spectroelectrochemical behavior of V_2O_5 thin films, the CV measurements were conducted within a potential range of -2 V to 2 V relative to Ag quasi-reference electrode with a scanning rate of 100 mV s^{-1} using a Biologic 3 channel potentiostat. Pt was used as a counter electrode in electrolyte 1 M $LiClO_4/PC$.

CHAPTER 3

RESULTS AND DISCUSSION

In this thesis, it is aimed to obtain V_2O_5 thin films over large areas using ultrasonic spray deposition method and thus to produce optoelectronic devices commercially. In order to better analyze the deposited thin films using ultrasonic spray pyrolysis method, the same characterization tests were conducted to the spin coated samples which were obtained at same conditions as ultrasonic spray deposited samples for comparison.

3.1. X-Ray Diffraction (XRD)

XRD patterns of the V_2O_5 thin films were used to investigate the crystallinity of the deposited films and determine their crystal structure. XRD results confirmed that crystal formation occurs following heat treatment. XRD patterns of V_2O_5 thin films deposited by spin coating and ultrasonic spray pyrolysis are provided in Figure 3. 1 and Figure 3. 2, respectively. When XRD patterns were examined, it was seen that untreated films produced by both methods show an amorphous structure. In accordance with similar studies in the literature [30][10][82][83][84], after annealing, all samples started to show a crystalline structure. All of the films showed an apparent diffraction peaks at $2\theta=20.34^\circ$ and 21.82° that can be attributed to the diffraction from (001) and (101) planes of V_2O_5 with orthorhombic (Pmmn) crystal structure (ICDS card #01-089-2482). All films had c-axis preferred orientation, the (001)-type planes lying parallel to the substrate. Besides that, V_2O_5 thin films deposited by ultrasonic spray pyrolysis contained two additional peaks at $2\theta=15.40^\circ$ and 31.06° indexed to (200) and (400) diffraction planes. They are also characteristic peaks of crystalline V_2O_5 . XRD patterns of films proved that the formation of crystalline V_2O_5 thin films. This crystallization of the films is of great importance in the electrochromic (EC)

properties of the films. Because EC performance depends on crystal structure due to the conduction of ions between the octahedral sites of crystalline V_2O_5 .

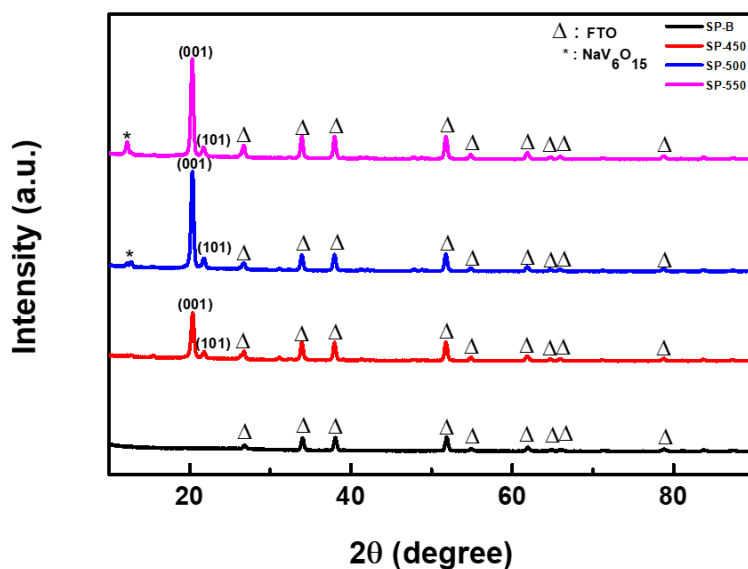


Figure 3. 1. XRD patterns of spin coated V_2O_5 films prepared at different annealing temperatures (a) as-deposited at room temperature, (b) 450 °C, (c) 500 °C and (d) 550 °C.

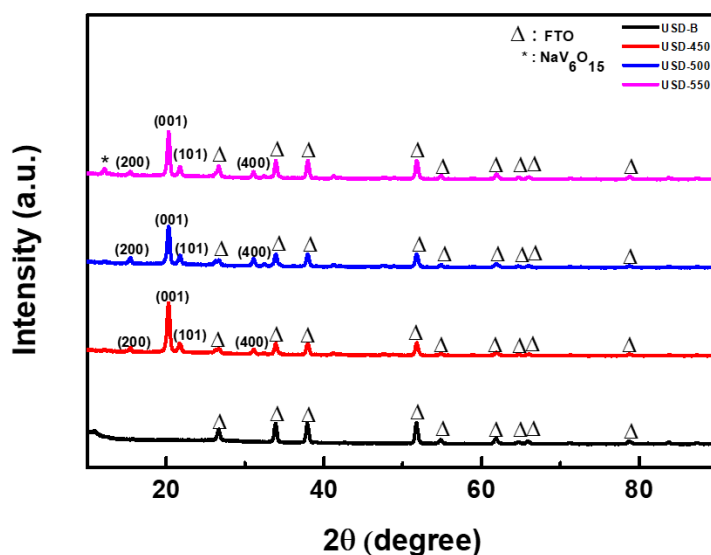


Figure 3. 2 XRD patterns of ultrasonic spray deposited V_2O_5 films prepared at different annealing temperatures (a) as-deposited at 100 °C, (b) 450 °C, (c) 500 °C and (d) 550 °C.

For the films annealed at 500 and 550 °C, patterns had an additional weak diffraction at an diffraction angle of $\sim 12.5^\circ$ denoted by star (*) is assigned to the formation $\text{NaV}_6\text{O}_{15}$. Intensity of the peak was found to increase with the annealing temperature from 500 to 550 °C. The formation of $\text{NaV}_6\text{O}_{15}$ can be explained by the diffusion of sodium (Na^+) ions from the glass substrate with increasing temperature during heat treatment [85].

3.2. Raman Spectroscopy

Raman spectra of V_2O_5 thin films deposited by two different methods and annealed at 450 °C are provided in Figure 3. 3. The peak positions for V_2O_5 is found to be in good agreement with the previous studies in literature [86][87][88] . The high-frequency Raman peak at 995 cm^{-1} is related with the vanadyl mode corresponding to the stretching of $\text{V}=\text{O}$, which results from unshared oxygen [89]. The presence of this peak proved the structural quality of the deposited V_2O_5 thin films. Peaks at 530 and 705 cm^{-1} are assigned to the stretching modes of the $\text{V}-\text{O}-\text{V}$ bridging bonds, the respective bending motions of these bonds attributed to the 304 and 483 cm^{-1} peaks. Peaks located at 283 and 406 cm^{-1} are assigned to the bending vibration of $\text{V}=\text{O}$ bonds [90]. However, Raman peaks at 145 and 197 cm^{-1} in low frequency region correspond to the lattice vibrations. These two peaks are completely related with the layered structure of V_2O_5 [91]. The peak at about 144 cm^{-1} is a rigid, layer-like mode [92]. The existence of this peak is an evidence of the layer-like structure of V_2O_5 films when the growth temperature is higher than 300 °C . This structure of V_2O_5 is established from distorted trigonal bipyramidal coordination polyhedra of oxygen atoms around vanadium atoms that share edges to form $(\text{V}_2\text{O}_4)_n$ zig-zag double chains along the (001) direction [93].

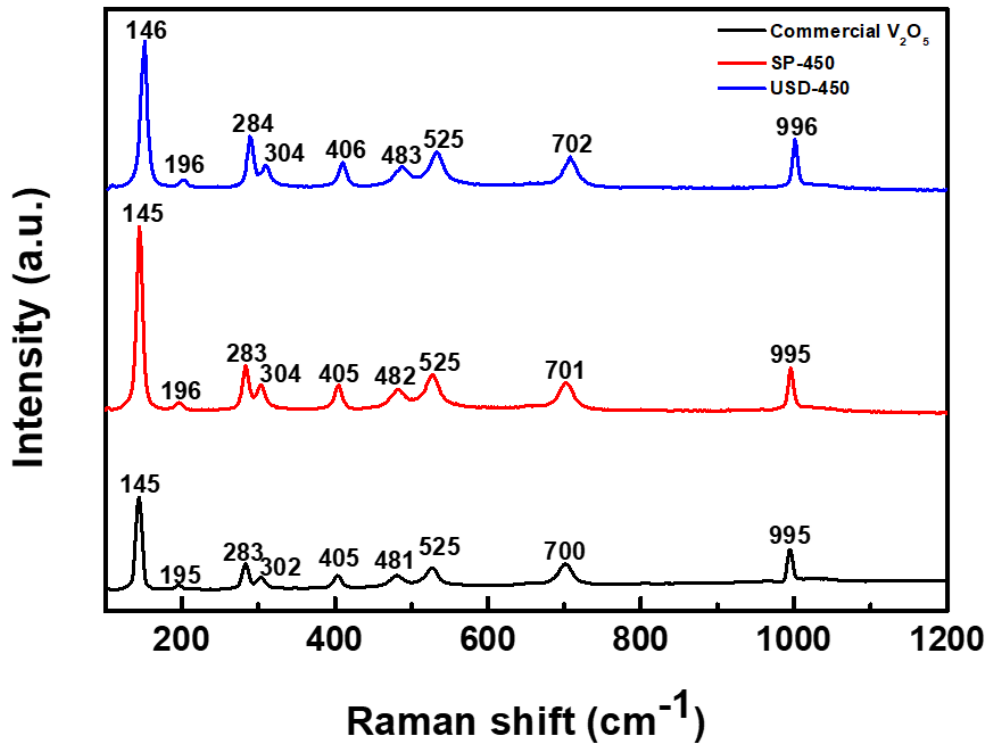


Figure 3. 3 Raman spectra of V₂O₅ thin films deposited by spin coating and ultrasonic spray pyrolysis methods.

Raman spectra of the samples are compared in Figure 3. 3. Raman spectrum for commercial V₂O₅ powder is also provided for comparison. When the effects of using two different methods on V₂O₅ thin films were investigated, a 1 cm⁻¹ shift in all the peaks of thin films deposited by ultrasonic spray pyrolysis. This shift in this mode is generally assigned to either the structural disorder or the stress developed in the film [93]. While samples were spin coated at room temperature, during spray coating, samples were located on a hot plate set at 100 °C. The faster removal of the precursor solution solvent from the film surface by the effect of induced temperature may have created stress in the structure of a thin film. This tensile stress might bring about a decrease in the interlayer distance.

3.3. X-Ray Photoelectron Spectroscopy (XPS)

XPS analysis was carried out to determine the oxidation state of Vanadium. XPS survey spectra is provided in Figure 3. 4. The survey spectra V_2O_5 displayed only the elements expected, together with carbon contamination for the oxides.

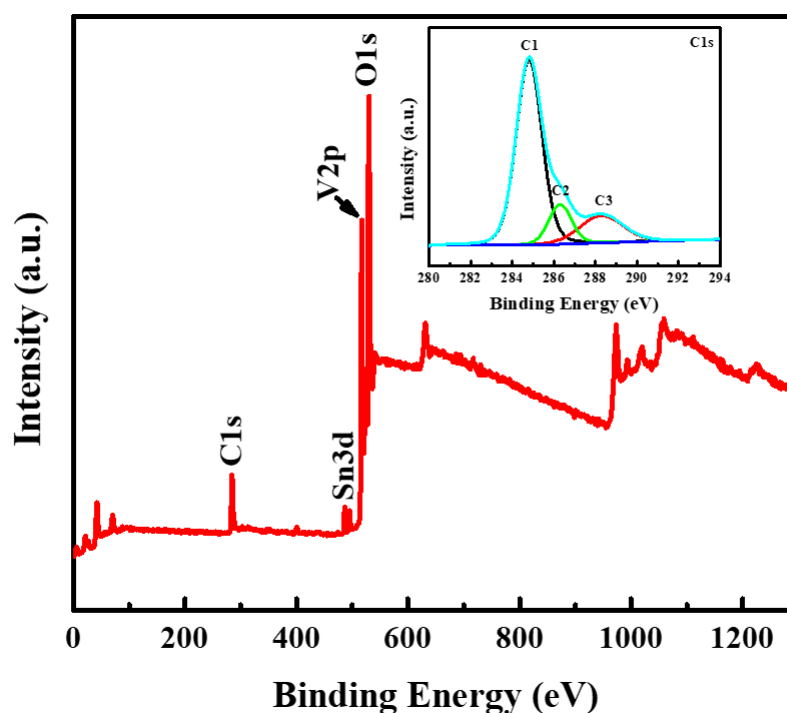


Figure 3. 4 Survey spectra of USD-450 sample. Insert shows C1s.

Regional XPS spectra of the V 2p and O 1s core levels are shown in the Figure 3. 5 (a) and (b), respectively. When C1s=284.68 eV was taken as a reference binding energy (BE), the O 1s was found at 529.99 eV that is in great agreement with the literature [94][95][96]. The BE of the oxygen is the most appropriate reference point since the ratio between oxygen and vanadium concentrations for different vanadium oxides. Besides, according to literature [94][97][98], the difference in binding energies between the O1s (VO_x) core level and the $V2p_{3/2}$ level ($\Delta = BE(O1s) - BE(V2p_{3/2})$) is one of the most useful parameters to determine the oxidation state of the vanadium. The $V2p_{3/2}$ of V_2O_5 was found at 516.9 eV and the Δ value for the V^{5+} ions coming from V 2p level is 13.09 eV for the USD-450 sample. Moreover, peak

widths for the metal and V(V) oxide are quite narrow, on the other hand the peak widths for V(III) and V(IV) oxides are considerably broadened.

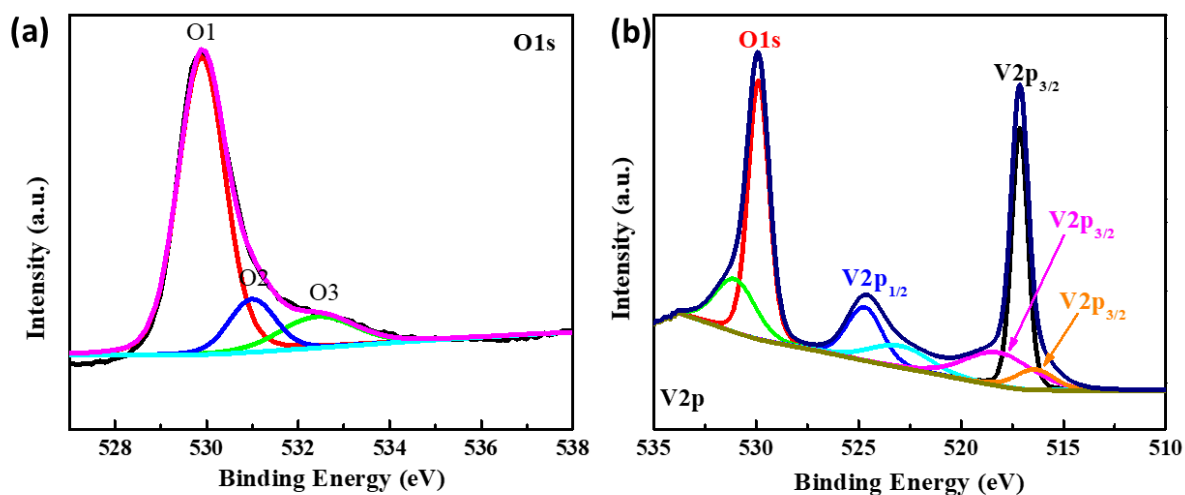


Figure 3. 5 XPS spectra for (a) O 1s and (b) V2p and core levels of the USD-450 sample.

The experimentally obtained fitting parameters are summarized in Table 3.1. These parameters are also compared to those in literature. It is confirmed that XPS analysis show the oxidation state of V_2O_5 .

Table 3. 1 XPS fit parameters for the $V2p_{3/2}$ and O1s peaks for vanadium oxide standards (Exp.*) and values reported in literature.

Vanadium oxide	E $V2p_{3/2}$ (eV)	FWHM $V2p_{3/2}$	E O1s (eV)	FWHM O1s	Δ (eV)	Ref.
V_2O_5	516.9	1.28	529.99	1.4	13.09	Exp.*
	516.9	1.6	529.8	1.7	12.9	[95]
	517.0	1.4	529.8	1.6	12.8	[94]
	517.2	1.2	-	-	-	[96]
	517.2	1.5	530.0	1.20	12.8	[97]

3.4. Scanning Electron Microscopy (SEM)

SEM analysis was carried out to investigate the surface morphology of the deposited V_2O_5 thin films. SEM images of spin coated thin films without annealing are given in Figure 3. 6 (a) and (b), and ultrasonic spray deposited films without annealing are given in Figure 3. 6 (c) and (d), respectively. Parallel to the XRD results, as-deposited films that were not annealed had amorphous structure. In contrast, USD-B sample had some features like crystallites.

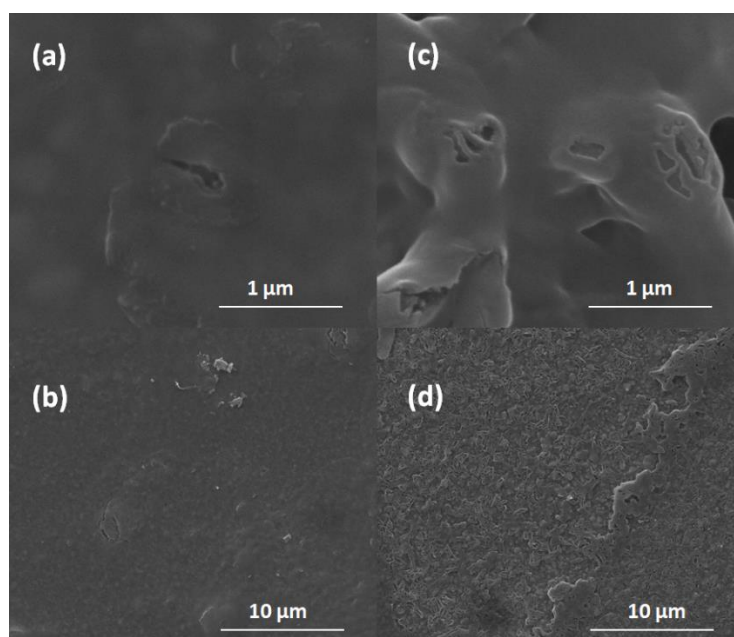


Figure 3. 6 Top view SEM micrographs of SP-B with different magnification (a) 120 000, (b) 15 000 and USD-B with different magnification (c) 120 000, (d) 15 000.

SEM images of spin coated samples annealed at 450, 500 and 500 °C with different magnifications are provided in Figure 3. 7 (a-b), (c-d) and (e-f), respectively. Moreover, ultrasonic spray deposited samples annealed at 450, 500 and 500 °C with different magnifications are provided in Figure 3. 8 (a-b), (c-d) and (e-f), respectively. It is clear that all of the films consist of nanorods that create homogeneously distributed pores without any cracks. Moreover, SEM images revealed that the particle sizes of the films produced by two different methods increase with annealing temperature. Films deposited through USP method had smoother surface as shown in

Figure 3.8 (e) and (f) upon annealing at 550 °C compared to spin coated counter parts. The SP-550 incorporates an uncontrolled cluster-grown rod-like feature as shown in Figure 3.7 (e) and (f).

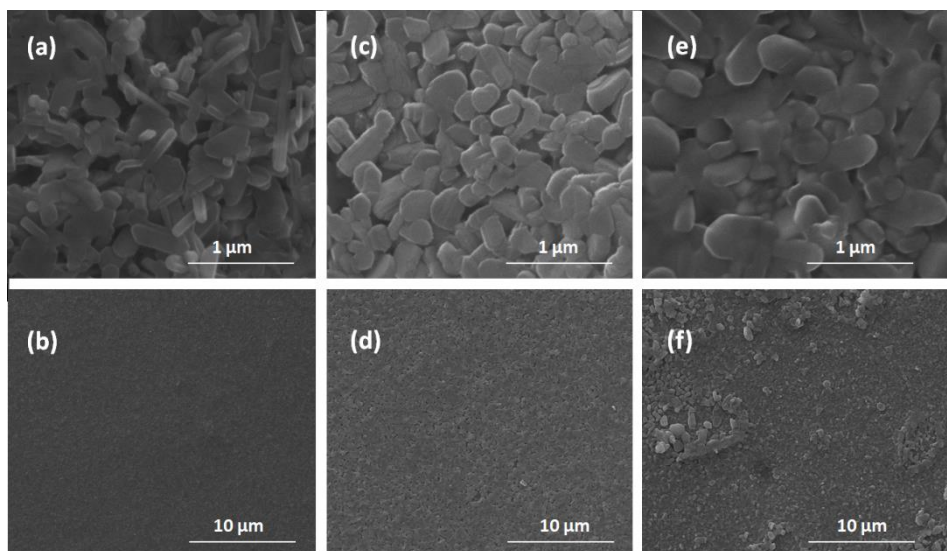


Figure 3. 7 Top view SEM micrographs of SP-450 with different magnification (a) 120 000, (b) 15 000, SP-500 with different magnification (c) 120 000, (d) 15 000 and SP-550 with different magnification (e) 120 000, (f) 15 000.

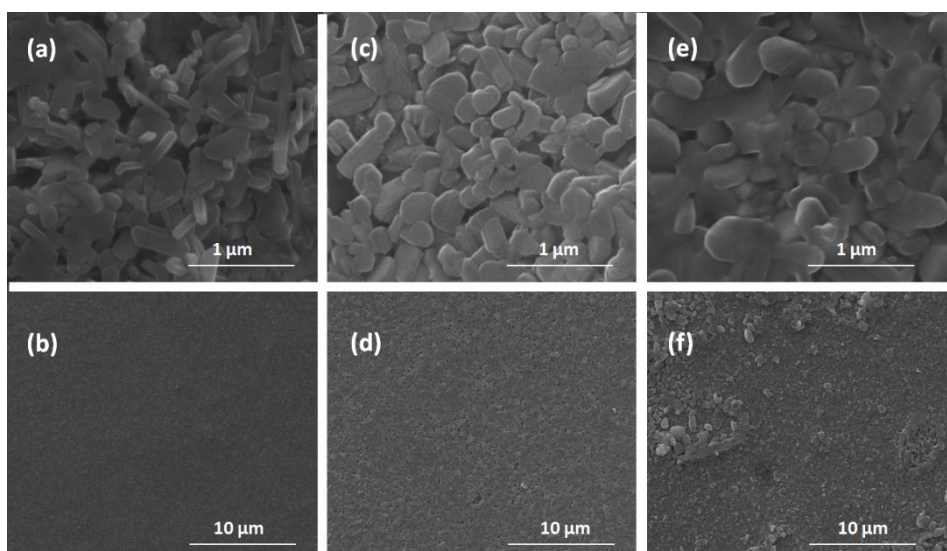


Figure 3. 8 Top view SEM micrographs of USD-450 with different magnification (a) 120 000, (b) 15 000, USD-500 with different magnification (c) 120 000, (d) 15 000 and USD-550 with different magnification (e) 120 000, (f) 15 000.

3.5. Atomic Force Microscopy (AFM)

Surface morphology and topography of the samples annealed at different temperatures were investigated using AFM images. Topographical AFM 3D images of the as-deposited SP-B and USD-B samples are provided in Figure 3. 9 (a) and (c), respectively. Also, AFM 2D images of SP-B and USD-B samples are provided in Figure 3. 9 (b) and (d), respectively. Similar to the SEM images, for the SP-B sample, no crystallites formation was observed due to its amorphous structure. However, USD-B sample showed some crystallites formation because of deposition at 100 °C even if it does not show a fully crystalline structure. Compared to the USD-B, surface of the SP-B was found to be very smooth due to its amorphous structure.

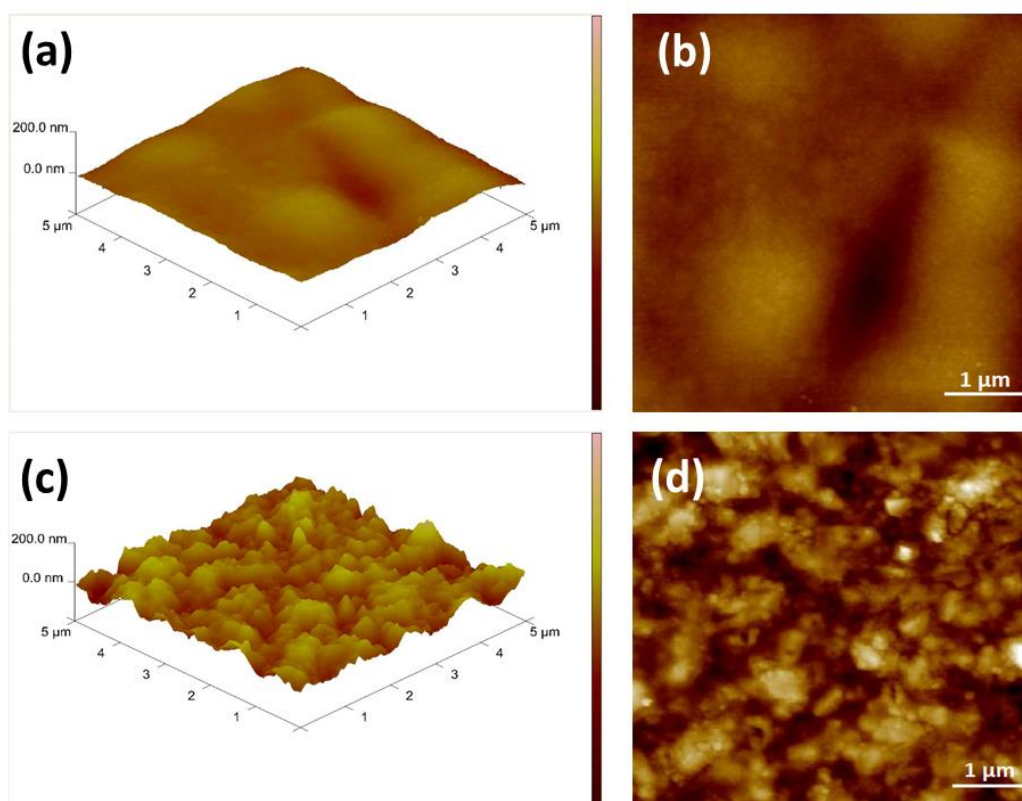


Figure 3. 9 Topographical AFM 3D images of the (a) SP-B, (c) USD-B samples and 2D images of the (b) SP-B, (d) USD-B samples.

Topographical AFM 3D images of the as-SP-450 and USD-450 samples are provided in Figure 3. 9 (a) and (c), respectively. Also, AFM 2D images of SP-450 and USD-

450 samples are provided in Figure 3. 910 (b) and (d), respectively . As evidenced by XRD analysis, AFM images also prove that a crystalline features started to be observed upon annealing at temperature above 300 °C. Moreover, USD-450 had a more rough surface with clear crystallites, in contrast to the spin coated sample.

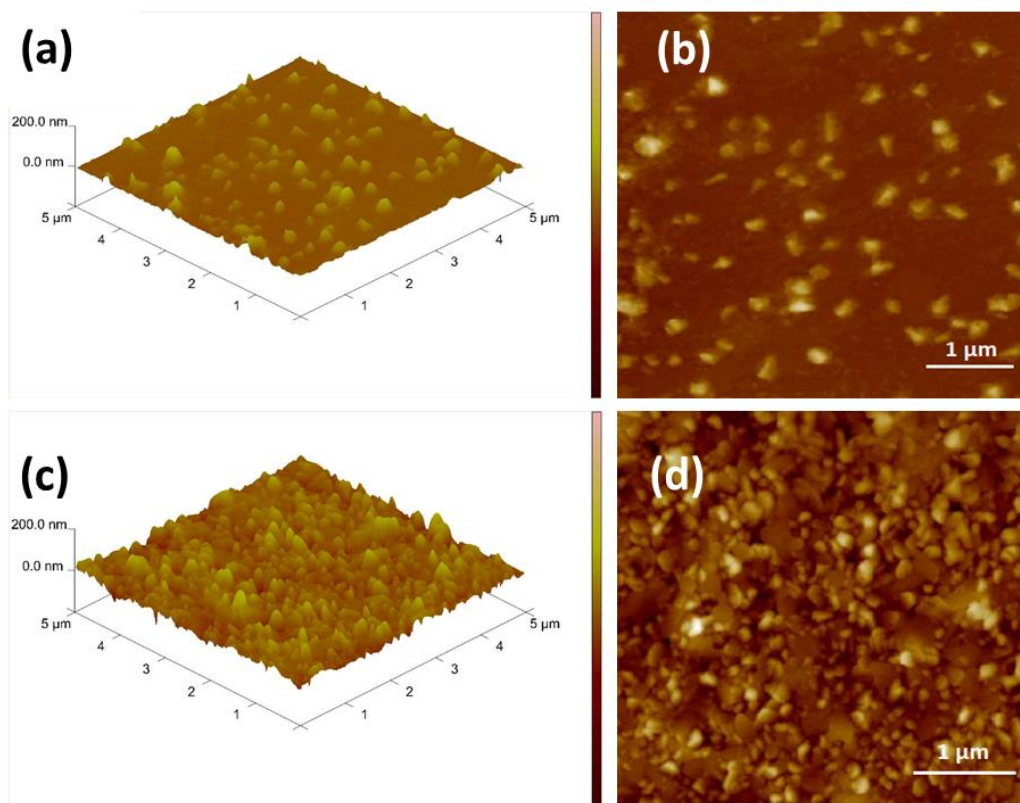


Figure 3. 10 Topographical AFM 3D images of the (a) SP-450, (c) USD-450 samples and 2D images of the (b) SP-450, (d) USD-450 samples.

Topographical AFM 3D images of SP-500, USD-500, SP-550 and USD-550 samples are provided in Figure 3. 11 (a),(c) and Figure 3. 12 (a),(c), respectively. Also, AFM 2D images of SP-500, USD-500, SP-550 and USD-550 samples are provided in Figure 3. 11 (b),(d) and Figure 3. 12 (b),(d), respectively. Nanorods with almost vertical orientation were found on all samples in agreement with SEM images. The effect of annealing temperature were apparent. Large grains proved that the particle size increases with the annealing temperature. As will be understood upon investigating

the optical properties, the temperature-dependent growth of the particles adversely affects the transmission[13]. For samples annealed at 550 °C, due to the high annealing temperature, crystallites were seen to be degraded and became tangled areas on the film surface.

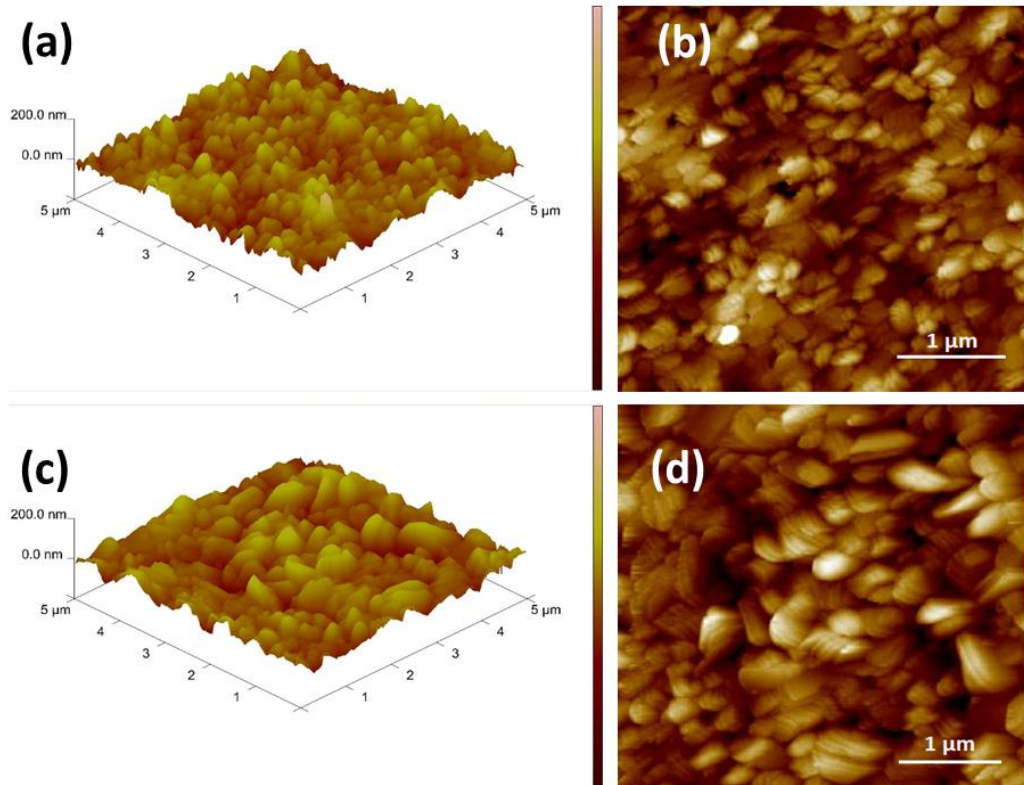


Figure 3. 11 Topographical AFM 3D images of the (a) SP-500, (c) USD-500 samples and 2D images of the (b) SP-500, (d) USD-500 samples .

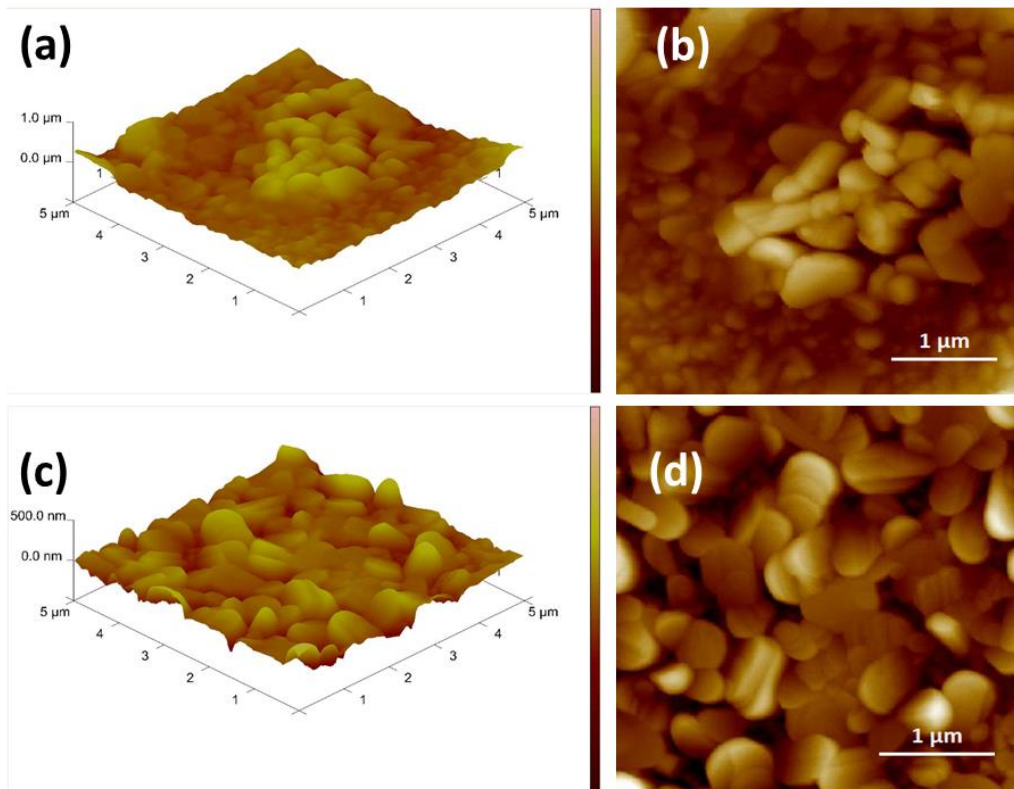


Figure 3. 12 Topographical AFM 3D images of the (a) SP-500, (c) USD-500 samples and 2D images of the (b) SP-500, (d) USD-500 samples.

Data obtained from AFM measurements are tabulated and provided in Table 3. 2. Roughness values of the samples were collected respective sampling sizes of $1 \times 1 \mu\text{m}$ and $200 \times 200 \text{ nm}$. In general, although the samples deposited by USP had a rougher surface, the USD-550 sample annealed at $550 \text{ }^\circ\text{C}$ was smoother than the SP-550 sample. Higher RMS roughness value in the V_2O_5 thin films obtained through USP method may be advantageous in EC devices since it provides a shorter diffusion path for the ions in the electrolyte [99]. Average grain sizes were also measured. Not surprisingly, with increasing the annealing temperature, grain size was found to gradually increase for all films following crystallization. Spin coated V_2O_5 thin films had smaller grain size. It might be beneficial for reversibility in EC performance since grain boundaries may take an active role as tunnels in electrolyte ion transfer.

Table 3. 2 R_a (average roughness), RMS (root mean square roughness) and average grain size values of each film.

Sample	R_a (nm)	RMS (nm)	Average Grain Size (nm)
SP-B	8.2 ± 2.3	10.8 ± 2.7	97.6
USD-B	16.7 ± 2.2	21.5 ± 2.4	195.0
SP-450	18.2 ± 2.9	22.8 ± 2.9	93.4
USD-450	19.6 ± 2.4	24.6 ± 2.3	185.0
SP-500	21.9 ± 1.8	25.1 ± 1.9	208.1
USD-500	29.6 ± 3.2	36.7 ± 3.7	284.0
SP-550	39.7 ± 2.9	49.2 ± 3.7	766.2
USD-550	31.5 ± 3.6	39.1 ± 3.5	491.4

3.6. X-Ray Fluorescence (XRF)

Thickness is one of the key parameters for deposition of thin films. It should be controlled through the amount of solution used and the number of coating repetitions because it has a very profound effect on optical properties. Fischer XDV-SDD XRF device was used for the thickness measurements. This instrument takes measurements from many points defined as matrix and gives a mean value, standard deviation, maximum and minimum values. When a material is exposed to X-Ray energy, which penetrates through the coating layer and the base material (depending on the type of the coating material and thickness), fluorescence energy is generated. The intensity (count rate) of this signal is directly proportional to the coating thickness. Sample thickness can be calculated by comparing it to a calibration curve that is generated by measuring standard material of similar composition and known thickness. Fundamental Parameters approach and Monte Carlo simulations can be used to obtain the calibration curve [100][101].

Measurement method was the same for all the samples and used a 6 x 3 matrix system. Data were collected from 18 points scattered in this matrix system at equal intervals. Obtained thickness of the samples was tabulated and provided in Table 3. 13. Considering that the spin-coated samples consist of 15 layers and the spray-coated samples consist of 12 layers, it can be stated that the thin films with similar thickness

can be obtained using less amount of solution in spray coating method. This is reasonable since spin coating is a quite wasteful method in terms of precursor solution. Furthermore, the thickness of all films was found to be approximately 50 nm, and it has been proved that thin films of the same thickness can be reproducibly obtained using the USD system. Coefficient of variation (COV) was also found below %5. It was indicated that deposited V₂O₅ thin films were highly homogeneous.

Table 3. 3 Thickness of the samples measured through XRF method.

Sample	Thickness of the Film (nm)	Standard Deviation (nm)
USD-B	50.1	2.5
USD-450	48.9	2.9
USD-500	50.9	2.9
USD-550	49.9	2.6
SP-B	48.7	2.7
SP-450	50.5	2.2
SP-500	51.2	2.7
SP-550	49.3	2.5

3.7. UV-Vis Spectrophotometry

Optical transmittance spectra of the spin coated and USD V₂O₅ thin films are provided in Figure 3. 13 (a) and (b), respectively, as a function of annealing temperature. Transmittance of SP-B sample was nearly 91%, whereas, that of SP-450, SP-500 and SP-550 samples are 86%, 76% and 74% , respectively within the wavelength range of 500-800nm. The same tendency was observed in samples deposited through USD method. The optical transmittance was 92% for the USD-B sample, while the transmittance for the other samples was 88%,79% and 75%, respectively. Optical transmittance was found be as-deposited films. In addition, in the near infrared region, a 5% increase in transmittance values of all films was observed. Although it is known that transmittance values increase with increasing substrate temperature, annealing temperature has an opposite effect [102]. It is thought that the increased grain size due to the annealing temperature would decrease the transmittance values of the films

[103]. Increasing roughness due to the temperature adversely affected the transmittance, in agreement with AFM and SEM results. When SP-550 and USD-550 samples are compared to contrary to the general trend, the overall transmittance of the USD-550, with a lower roughness, is found to be higher. This results shows that they are in strong agreement with each other.

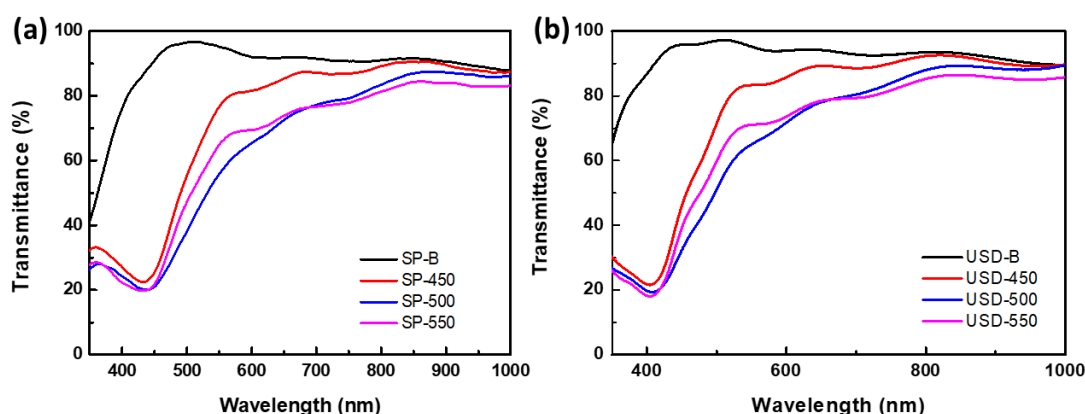


Figure 3. 13 Transmittance spectra for V_2O_5 thin films deposited by (a) spin coating method and (b) USD method.

Optical band gap of the deposited thin films can be calculated using Tauc plots provided in Figure 3.14 in conjunction with the following equation:

$$\alpha h\nu = A (h\nu - E_g)^{n/2}$$

,where α is the absorption coefficient, ν is the light frequency, A is a constant and E_g is the band gap. n is an index and determines the type of band gap as a direct or indirect. The variation of $(\alpha h\nu)^2$ versus $h\nu$ for V_2O_5 thin films, known as Tauc plot (Figure 3. 14) was used to obtain the direct band gap of these films was obtained by the extrapolation of the straight line part of the graph. Optical band gaps for SP-450, SP-500 and SP-550 were estimated as 2.52, 2.44 and 2.34 eV, respectively. Similarly, USD-450, USD-500 and USD-550 samples have band gaps of 2.66, 2.62 and 2.57 eV, respectively. These band gap values coincidence with the previous studies.

Furthermore, obviously, as the annealing temperature increases, optical bandgaps of the films decrease. This change can be attributed to the presence of structural defects such as grain boundaries.

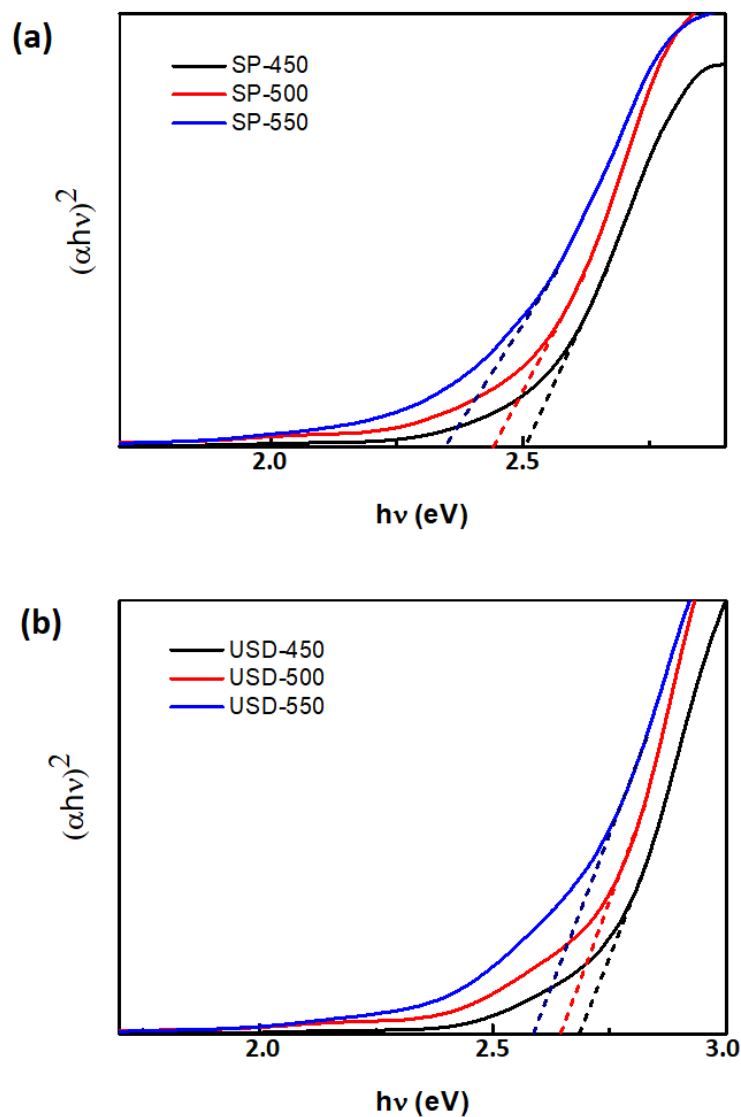


Figure 3. 14 Tauc plots for (a) spin coated and (b) USD deposited V_2O_5 thin films annealed at 450, 500 and 550 °C.

Transmittance changes of the USD samples with potential range of 2 to -2 V in electrolyte 1M LiClO₄/PC was recorded and provided in Figure 3. 15. For as-deposited USD film, there was no change in the transmittance as expected since electrochromic response is only reported for orthorhombic crystalline structure [62][63]. At a wavelength of 800 nm, a maximum transmittance change 12% was obtained for USD-450. USD-500 and USD-550 samples showed maximum change at similar wavelengths and these changes were found to be only 5% and 4% , respectively. Moreover, the transmittance change in the USD-500 sample was not observed below 600 nm, while the change of USD-550 remains constant within the 650-1000 nm range. In this respect, the USD-550 sample showed similar response with the USD-450 sample. The low degree of variation in the transmittance of the samples can be explained by the low film thickness. As the thickness of the films increase, a significant transmittance change is expected.

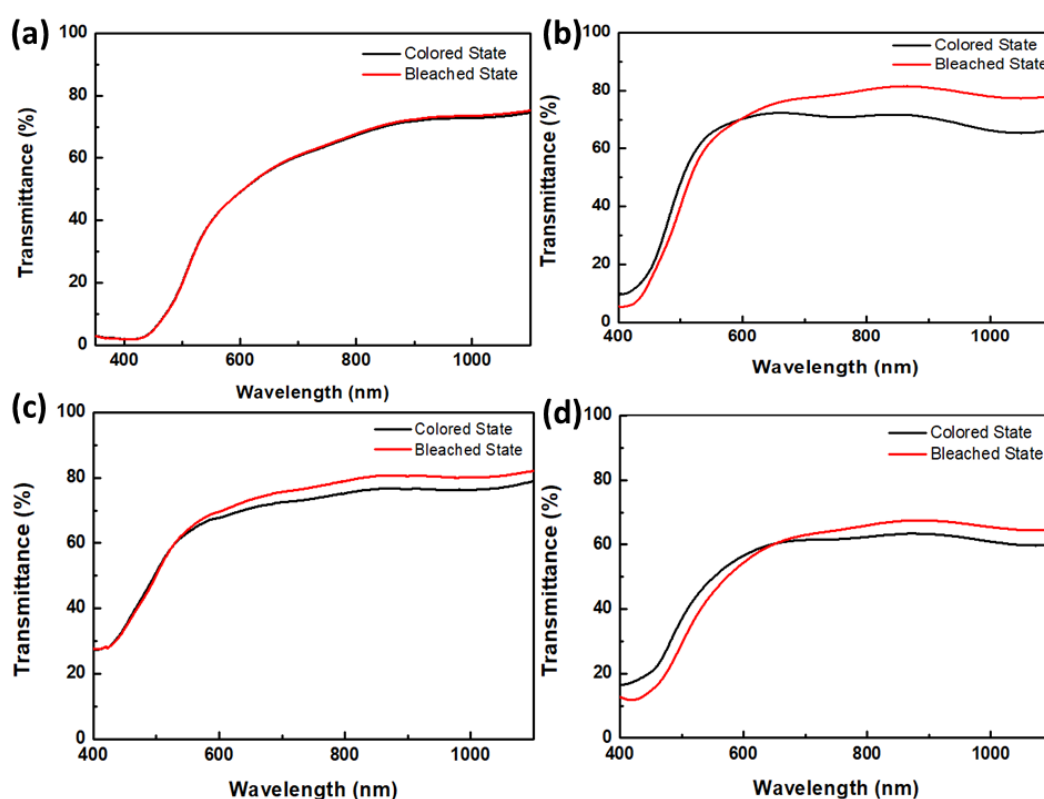
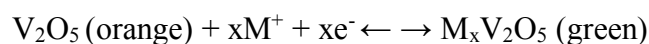


Figure 3. 15 Transmittance spectra for (a) USD-B, (b) USD-450, (c) USD-500 and (d) USD-550 samples in colored and bleached states.

3.8. Cyclic Voltammetry

The electrochromism of V_2O_5 film can be considered as a reversible reduction-oxidation process accompanying the double injection extraction of Li^+ ions and electrons [104] :



M: H, Li, Na or K ions

As an initial step, cyclic voltammetry measurements were carried out to investigate this reversible redox process. Cyclic voltammograms of the SP-450 and USD-450 samples are provided in Figure 3. 16 (a) and (b), respectively. CV analysis was conducted within the applied potential range of -2 to 2 V relative to Ag/AgCl reference electrode at a scanning rate of 100 mVs^{-1} . Pt was used as counter electrode and 1M $LiClO_4/PC$ was used as the electrolyte. It is possible to observe the presence of two oxidation states, one at 0.18 V and another at 0.60 V for both samples. The first is due to the oxidation of part of the vanadium sites (+4) to vanadium (+5). The second oxidation peak corresponds to the oxidation in the remaining vanadium sites (+4) for the state of oxidation +5 [105].

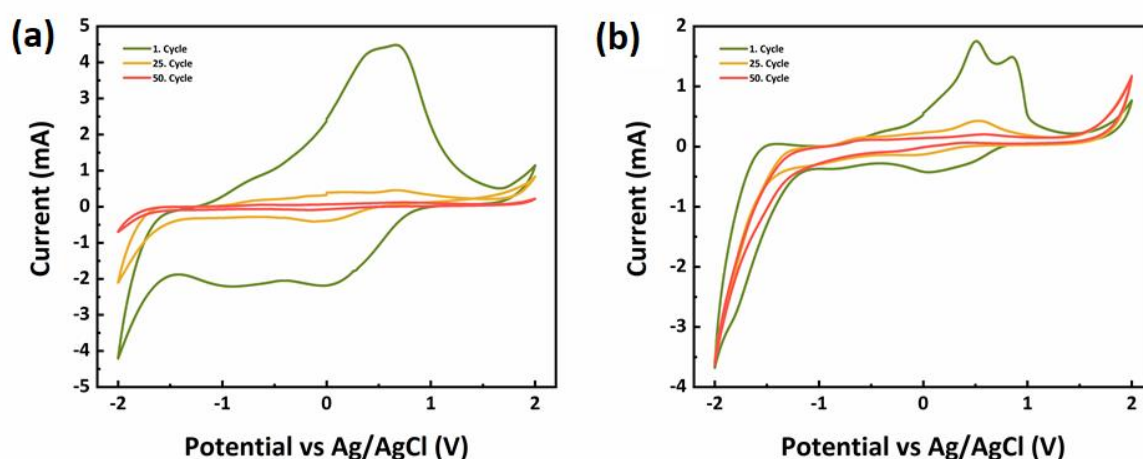


Figure 3. 16 CV results of (a) SP-450 and (b) USD-450 samples.

These films exhibited higher current density initially and the current density was found to decrease gradually up to the 50th cycle, where eventually the films lost their EC response. Then, V₂O₅ particles was observed within the electrolyte. This indicated that there is a significant stability problem arising from the adhesion of V₂O₅ thin film to the FTO surface. Some functional polymer binders like poly(acrylic acid) (PAA), poly(methacrylic acid) (PMA), and poly(vinyl alcohol) (PVA) have been reported in literature for the reversible lithium intercalation [106]. In order to overcome the stability problem, it was decided to use PMMA as an alternative binder and the surface of the USD-450 sample was coated with a few nanometers thick PMMA layer using spin coating. CV result of PMMA coated USD-450 sample is provided in . Other CV parameters being the same, the color of the film was observed to be green at -0.3 V and orange at +1.9 V in accordance with the literature [106]. Up to 200th cycle, film showed excellent reversibility upon the deposition of PMMA layer.

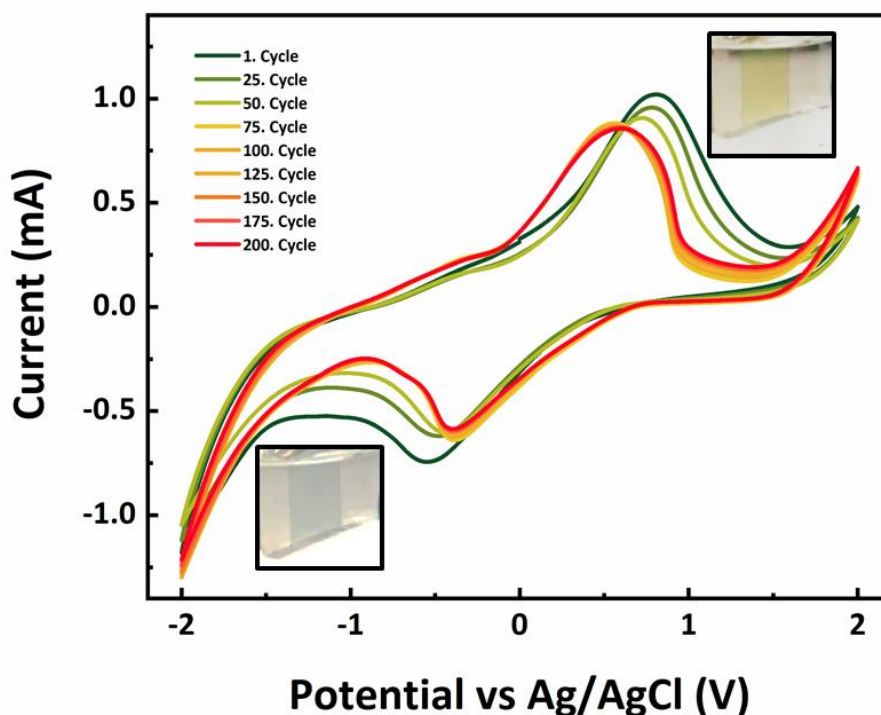


Figure 3. 17 CV result of the PMMA coated USD-450 sample. Inserts show the photographs of the colored thin films at respective potentials

CHAPTER 4

CONCLUSIONS AND FUTURE RECOMMENDATIONS

V₂O₅ thin films were deposited onto FTO coated glass substrates by spin coating and ultrasonic spray pyrolysis method. Annealing was applied to the films at different temperatures of 450, 500 and 550 °C. Following annealing, homogeneous and uniform crystalline thin films were obtained with orthorhombic crystal structure.

Structural and morphological analyses revealed that films were composed of single V₂O₅ phase and annealing temperature had a great impact on the grain size of the films. It was observed that the particle size increase gradually with the annealing temperature. Accordingly, the roughness of the films was increased.

Upon examination of the optical properties, it was seen that the transmittance values of the films got adversely affected by the increased annealing temperature. Films were transparent in the visible region of the spectrum and their transmittance decreased from 88 to 75% upon increasing the annealing temperature from 450 to 550 °C, respectively. Optical band gap values of the films were determined from Tauc plot which were in the range of 2.34 – 2.66 eV. It was clearly seen that as the applied annealing temperature increases, optical bandgaps of the films were found to decrease with the increased annealing temperatures.

Films showed EC response within the applied potential range of -2 to 2 V. The transmittance changes of the USD-450, USD-500 and USD-550 samples are 10, 5 and 4%, respectively. It is believed that the changes in optical transmittance values and thus the optical contrast can be improved with increased film thickness. Furthermore, V₂O₅ thin films were green in the bleached state and orange in the colored state. Films had good chemical reversibility; but their EC stability was very problematic due to the poor adhesion to the surface. PMMA coating was utilized as a binder on to of V₂O₅

thin films and significant stability improvement was obtained for the investigated 200 cycles.

The process based findings provided in this thesis provide a road map for the ultrasonic spray deposition of V_2O_5 thin films. USD method can be practiced over large areas suitable for the fabrication of optoelectronic devices in commercial sizes. Electrochromic devices were investigated in this work as a starting point in this regard. An adhesion based stability problem was experienced, which was overcome by a binder layer coated directly on V_2O_5 thin films. This indicated that a full EC device with gel electrolyte will provide a permanent solution to the stability problems. As stated earlier, thickness of V_2O_5 thin films have to be increased for obtaining higher optical contrast. Therefore, a much more systematic study on the use of USD deposited V_2O_5 thin films is required.

In parallel, the USD deposited V_2O_5 thin films can be utilized in solar cells. Prior to this, though, carrier type, concentration, mobility and a valance band and conduction band edges of the deposited films should be determined systematically.

REFERENCES

- [1] D. A. Jameel, "Thin Film Deposition Processes," *MRS Bull.*, vol. 1, no. 4, pp. 193–199, 2015.
- [2] O. Oluwatosin Abegunde, E. Titilayo Akinlabi, O. Philip Oladijo, S. Akinlabi, and A. Uchenna Ude, "Overview of thin film deposition techniques," *AIMS Mater. Sci.*, vol. 6, no. 2, pp. 174–199, 2019.
- [3] X. Hu, "Production technology and application of thin film materials in micro fabrication," no. Mmebc, pp. 1193–1199, 2016.
- [4] D. M. Mattox, *Physical Sputtering and Sputter Deposition (Sputtering)*. 2009.
- [5] G. Bahuguna, N. K. Mishra, P. Chaudhary, A. Kumar, and R. Singh, "Thin Film Coating through Sol-Gel Gel Technique," *Res. J. Chem. Sci.*, vol. 6, no. June, pp. 65–72, 2016.
- [6] A. I. G. Varela, M. Aymerich, D. N. García and Y. C. Martín, "Sol-Gel Glass Coating Synthesis for Different Applications: Active Gradient-Index Materials, Microlens Arrays and Biocompatible Channels," *Recent Appl. Sol-Gel Synth.*, 2017
- [7] R. Denk, M. Geissert, M. Hieber, J. Saal, and O. Sawada, "The spin-coating process: Analysis of the free boundary value problem," *Commun. Partial Differ. Equations*, vol. 36, no. 7, pp. 1145–1192, 2011.
- [8] L. A. Dobrzański and M. Szindler, "Sol gel TiO₂ antireflection coatings for silicon solar cells," no. May 2012, 2015.
- [9] T. Guo, M. S. Yao, Y. H. Lin, and C. W. Nan, "A comprehensive review on synthesis methods for transition-metal oxide nanostructures," *CrystEngComm*, vol. 17, no. 19, pp. 3551–3585, 2015.
- [10] D. Hou, Y. Lu, and F. Song, "Effects of substrate temperature on properties of vanadium oxide thin films on Si substrate," *Second Int. Conf. Photonics Opt. Eng.*, vol. 10256, no. February 2017, p. 102560R, 2017.
- [11] R. H. Bari, S. B. Patil, and A. R. Bari, "Spray Pyrolysed Prepared CuO–ZnO Nanocomposites Thin Films for Ethanol Sensor," *Mater. Focus*, vol. 3, no. 2, pp. 119–124, 2014.

- [12] M. M. Margoni, S. Mathuri, K. Ramamurthi, R. R. Babu, and K. Sethuraman, "Investigation on the pure and fluorine doped vanadium oxide thin films deposited by spray pyrolysis method," *Thin Solid Films*, vol. 606, pp. 51–56, 2016.
- [13] D. Huang, Y. Gong, B. Liu, Q. Zhao, and X. Zhao, "Effect of annealing temperature on the structure and properties of titanium oxide films," *Wuhan Ligong Daxue Xuebao/Journal Wuhan Univ. Technol.*, vol. 24, no. 6, p. 1, 2002.
- [14] S. M. Sabnis, "Process flow of spray pyrolysis technique," *IOSR J. Appl. Phys.*, vol. 4, no. 5, pp. 07–11, 2013.
- [15] L. Filipovic, S. Selberherr, G. C. Mutinati, E. Brunet and S. Steinhauer, "A method for simulating spray pyrolysis deposition in the level set framework," *Eng. Lett.*, vol. 21, no. 4, pp. 224–240, 2013
- [16] A. J. Kelly, "Charge injection electrostatic atomizer modeling," *Aerosol Sci. Technol.*, vol. 12, no. 3, pp. 526–537, 1990.
- [17] L. J. Gauckler and D. Perednis, "Thin Film Deposition Using Spray Pyrolysis," *J. Electroceramics*, vol. 14, no. March 2005, pp. 103–111, 2004.
- [18] A. Chakrabarti, K. Hermann, R. Druzinic, M. Witko, F. Wagner, and M. Petersen, "Geometric and electronic structure of vanadium pentoxide: a density functional bulk and surface study," *Phys. Rev. B - Condens. Matter Mater. Phys.*, vol. 59, no. 16, pp. 10583–10590, 1999.
- [19] S. L. McArthur, "Thin films of Vanadium Oxide Grown on Vanadium metal," *Surf. Interface Anal.*, vol. 38, no. c, pp. 1380–1385, 2006.
- [20] S. Krishnakumar and C. S. Menon, "Optical and electrical properties of vanadium pentoxide thin films," *Phys. Status Solidi Appl. Res.*, vol. 153, no. 2, pp. 439–444, 1996.
- [21] J. Yao, Y. Li, R. C. Massé, E. Uchaker, and G. Cao, "Revitalized interest in vanadium pentoxide as cathode material for lithium-ion batteries and beyond," *Energy Storage Mater.*, vol. 11, no. June 2017, pp. 205–259, 2018.
- [22] C. V. Ramana, O. M. Hussain, R. Pinto, and C. M. Julien, "Microstructural features of pulsed-laser deposited V₂O₅ thin films," *Appl. Surf. Sci.*, vol. 207, no. 1–4, pp. 135–138, 2003.
- [23] J. P. Audiere, A. Madi, and J. C. Grenet, "Electrical and thermal properties of

- highly quenched amorphous V_2O_5 thin films,” *J. Mater. Sci.*, vol. 17, no. 10, pp. 2973–2978, 1982.
- [24] N. Kumagai, H. Kitamoto, M. Baba, S. Durand-Vidal, D. Devilliers, and H. Groult, “Intercalation of lithium in r.f.-sputtered vanadium oxide film as an electrode material for lithium-ion batteries,” *J. Appl. Electrochem.*, vol. 28, no. 1, pp. 41–48, 1998.
- [25] M. Benmoussa, A. Outzourhit, R. Jourdani, A. Bennouna, and E. L. Ameziane, “Structural, optical and electrochromic properties of sol-gel V_2O_5 thin films,” *Act. Passiv. Electron. Components*, vol. 26, no. 4, pp. 245–256, 2003.
- [26] C. Julien, E. Haro-Poniatowski, M. A. Camacho-López, L. Escobar-Alarcón, and J. Jiménez-Jarquín, “Growth of V_2O_5 thin films by pulsed laser deposition and their applications in lithium microbatteries,” *Mater. Sci. Eng. B Solid-State Mater. Adv. Technol.*, vol. 65, no. 3, pp. 170–176, 1999.
- [27] M. Losurdo, D. Barreca, G. Bruno, and E. Tondello, “Spectroscopic ellipsometry investigation of V_2O_5 nanocrystalline thin films,” *Thin Solid Films*, vol. 384, no. 1, pp. 58–64, 2001.
- [28] Guimond, S., Sturm, J. M., Göbke, D., Romanyshyn, Y., Naschitzki, M., Kühlenbeck, H. and Freund, H. J. , “Well-ordered V_2O_5 (001) thin films on Au (111): Growth and thermal stability,” *J. Phys. Chem. C*, vol. 112, no. 31, pp. 11835–11846, 2008.
- [29] A. B. Cezar, I. L. Graff, J. Varalda, W. H. Schreiner, and D. H. Mosca, “Oxygen-vacancy-induced room-temperature magnetization in lamellar V_2O_5 thin films,” *J. Appl. Phys.*, vol. 116, no. 16, 2014.
- [30] N. Özer, “Electrochemical properties of sol-gel deposited vanadium pentoxide films,” *Thin Solid Films*, vol. 305, no. 1–2, pp. 80–87, 1997.
- [31] C. V. Ramana, O. M. Hussain, B. S. Naidu, C. Julien, and M. Balkanski, “Physical investigations on electron-beam evaporated vanadium pentoxide films,” *Mater. Sci. Eng. B*, vol. 52, no. 1, pp. 32–39, 1998.
- [32] A. Kumar, P. Singh, N. Kulkarni, and D. Kaur, “Structural and optical studies of nanocrystalline V_2O_5 thin films,” *Thin Solid Films*, vol. 516, no. 6, pp. 912–918, 2008.
- [33] S. Senapati and S. Panda, “Effect of aging of V_2O_5 sol on properties of nanoscale films,” *Thin Solid Films*, vol. 599, pp. 42–48, 2016.

- [34] P. Rosaiah, G. L. Sandhya, S. Suresh, J. Zhu, Y. Qiu, and O. M. Hussain, "Effect Of Substrate Temperature On Micro-structural, Optical And Electrical Properties Of V₂O₅ Thin Films," *Adv. Mater. Proc.*, vol. 1, no. 2, pp. 215–219, 2016.
- [35] R. Santos, J. Loureiro, A. Nogueira, E. Elangovan, J. V. Pinto and J. P. Veiga, "Thermoelectric properties of V₂O₅ thin films deposited by thermal evaporation," *Appl. Surf. Sci.*, vol. 282, pp. 590–594, 2013.
- [36] H. Q. Wang, N. Li, N. S. Guldal, and C. J. Brabec, "Nanocrystal V₂O₅ thin film as hole-extraction layer in normal architecture organic solar cells," *Org. Electron.*, vol. 13, no. 12, pp. 3014–3021, 2012.
- [37] C. V. Ramana and O. M. Hussein, "Optical absorption behaviour of vanadium pentoxide thin films," *Adv. Mater. Opt. Electron.*, vol. 7, no. 5, pp. 225–231, 1997.
- [38] J. M. Cocciantelli *et al.*, "On the $\delta \rightarrow \gamma$ irreversible transformation in Li// V₂O₅ secondary batteries," *Solid State Ionics*, vol. 78, no. 1–2, pp. 143–150, 1995.
- [39] A. Lourenço, A. Gorenstein, S. Passerini, W. H. Smyrl, M. C. A. Fantini, and M. H. Tabacniks, "Radio-frequency reactively sputtered VO_x thin films deposited at different oxygen flows," *J. Electrochem. Soc.*, vol. 145, no. 2, pp. 706–711, 1998.
- [40] D. Manno, A. Serra, M. Di Giulio, G. Micocci, A. Taurino, A. Tepore and D. Berti, "Structural and electrical properties of sputtered vanadium oxide thin films for applications as gas sensing material," *J. Appl. Phys.*, vol. 81, no. 6, pp. 2709–2714, 1997
- [41] G. Y. Song, C. Oh, S. Sinha, J. Son, and J. Heo, "Facile Phase Control of Multivalent Vanadium Oxide Thin Films (V₂O₅ and VO₂) by Atomic Layer Deposition and Postdeposition Annealing," *ACS Appl. Mater. Interfaces*, vol. 9, no. 28, pp. 23909–23917, 2017.
- [42] R. Irani, S. M. Rozati, and S. Beke, "Structural and optical properties of nanostructural V₂O₅ thin films deposited by spray pyrolysis technique: Effect of the substrate temperature," *Mater. Chem. Phys.*, vol. 139, no. 2–3, pp. 489–493, 2013.
- [43] Z. Yong, Y. Liu, "Electrochemical impedance spectra of V₂O₅ xerogel films with intercalation of lithium ion" *J. Cent. South Univ. Technol.* vol. 12, no. 3,

pp. 2–3, 2005.

- [44] C. Julien, A. Khelifa, J. P. Guesdon, V. Tuncheva, and F. Gendron, “Electrical properties of flash-evaporated V_2O_5 films,” *Ionics (Kiel)*, vol. 2, no. 5–6, pp. 380–385, 1996.
- [45] C. Sanchez, J. Livage, J. P. Audiere and A. Madi, “Influence of the quenching rate on the properties of amorphous V_2O_5 thin films,” *J. Non. Cryst. Solids*, vol. 65, no. 2–3, pp. 285–300, 1984.
- [46] Z. Luo, Z. Wu, X. Xu, M. Du, T. Wang, and Y. Jiang, “Impact of substrate temperature on the microstructure, electrical and optical properties of sputtered nanoparticle V_2O_5 thin films,” *Vacuum*, vol. 85, no. 2, pp. 145–150, 2010.
- [47] A. Mauger and C. M. Julien, “ V_2O_5 thin films for energy storage and conversion,” *AIMS Mater. Sci.*, vol. 5, no. 3, pp. 349–401, 2018.
- [48] S. Zhuiykov, W. Wlodarski, and Y. Li, “Nanocrystalline V_2O_5 - TiO_2 thin-films for oxygen sensing prepared by sol-gel process,” *Sensors Actuators, B Chem.*, vol. 77, no. 1–2, pp. 484–490, 2001.
- [49] D. W. Murphy, P. A. Christian, F. J. Disalvo, and J. V. Waszczak, “Lithium Incorporation by Vanadium Pentoxide,” *Inorg. Chem.*, vol. 18, no. 10, pp. 2800–2803, 1979.
- [50] L. T. Zhang, J. Song, Q. F. Dong, and S. T. Wu, “Application of V_2O_5 in Thin Film Microbatteries Prepared by RF Magnetron Sputtering,” *Adv. Mater. Res.*, vol. 79–82, pp. 931–934, 2009.
- [51] J. B. Bates, N. J. Dudney, D. C. Lubben, G. R. Gruzalski, B. S. Kwak, X. Yu and R. A. Zuhr, “Thin-film rechargeable lithium batteries,” *J. Power Sources*, vol. 54, no. 1, pp. 58–62, 1995.
- [52] K. Le Van, H. Groult, A. Mantoux, L. Perrigaud, F. Lantelme and R. Lindström, “Amorphous vanadium oxide films synthesised by ALCVD for lithium rechargeable batteries,” *J. Power Sources*, vol. 160, no. 1, pp. 592–601, 2006.
- [53] C. V. Ramana, O. M. Hussain, S. Uthanna, and B. S. Naidu, “Influence of oxygen partial pressure on the optical properties of electron beam evaporated vanadium pentoxide thin films,” *Opt. Mater. (Amst)*, vol. 10, no. 2, pp. 101–107, 1998.
- [54] M. Ponzi, C. Duschatzky, A. Carrascull, and E. Ponzi, “Obtaining

- benzaldehyde via promoted V_2O_5 catalysts,” *Appl. Catal. A Gen.*, vol. 169, no. 2, pp. 373–379, 1998.
- [55] R. J. Colton, A. M. Guzman, and J. W. Rabalais, “Photochromism and Electrochromism in Amorphous Transition Metal Oxide Films,” *Acc. Chem. Res.*, vol. 11, no. 4, pp. 170–176, 1978.
- [56] N. Guru Prakash, M. Dhananjaya, B. Purusottam Reddy, K. Sivajee Ganesh, A. Lakshmi Narayana, and O. M. Hussain, “Molybdenum doped V_2O_5 Thin Films electrodes for Supercapacitors,” *Mater. Today Proc.*, vol. 3, no. 10, pp. 4076–4081, 2016.
- [57] M. A. Sutar, M. S. Pawar, M. K. Rendale, and S. G. Kandalkar, “Enhancing Electrochemical Performance of V_2O_5 Thin Film by using Ultrasonic Weltering,” vol. 7, no. 6, pp. 41–45, 2015.
- [58] G. L. Sandhya, M. Dhananjaya, N. Guruprakash, A. Lakshminarayana, P. Rosaiah, and O. M. Hussain, “Structural And Supercapacitive Performance Of V_2O_5 Thin Films Prepared By DC Magnetron Sputtering,” *IOSR J. Appl. Chem.*, vol. 10, no. 05, pp. 64–69, 2017.
- [59] G. Rizzo, A. Arena, A. Bonavita, N. Donato, G. Neri, and G. Saitta, “Gasochromic response of nanocrystalline vanadium pentoxide films deposited from ethanol dispersions,” *Thin Solid Films*, vol. 518, no. 23, pp. 7124–7127, 2010.
- [60] M. Abbasi, S. M. Rozati, R. Irani, and S. Beke, “Synthesis and gas sensing behavior of nanostructured V_2O_5 thin films prepared by spray pyrolysis,” *Mater. Sci. Semicond. Process.*, vol. 29, pp. 132–138, 2015.
- [61] G. Micocci, A. Serra, A. Tepore, S. Capone, R. Rella, and P. Siciliano, “Properties of vanadium oxide thin films for ethanol sensor,” *J. Vac. Sci. Technol. A Vacuum, Surfaces, Film.*, vol. 15, no. 1, pp. 34–38, 1997.
- [62] J. Huotari, R. Bjorklund, J. Lappalainen, and A. Lloyd Spetz, “Pulsed Laser Deposited Nanostructured Vanadium Oxide Thin Films Characterized as Ammonia Sensors,” *Sensors Actuators, B Chem.*, vol. 217, pp. 22–29, 2015.
- [63] D. Raj, D. Mangalaraj, N. Ponpandian, and J. Yi, “Gas sensing properties of chemically synthesized V_2O_5 thin films,” *Adv. Mater. Res.*, vol. 123–125, no. 2, pp. 683–686, 2010.
- [64] Y. Vijayakumar, G. K. Mani, M. V. R. Reddy, and J. B. B. Rayappan,

- “Nanostructured flower like V_2O_5 thin films and its room temperature sensing characteristics,” *Ceram. Int.*, vol. 41, no. 2, pp. 2221–2227, 2015.
- [65] K. Schneider, M. Lubecka, and A. Czapla, “ V_2O_5 thin films for gas sensor applications,” *Sensors Actuators, B Chem.*, vol. 236, pp. 970–977, 2016.
- [66] EPA, “Toxicological Review of Vanadium Pentoxide,” *Rev. Lit. Arts Am.*, vol. 39, no. 110, pp. 759–786, 2010.
- [67] I. Mjejri, L. M. Manceri, M. Gaudon, A. Rougier, and F. Sediri, “Nano-vanadium pentoxide films for electrochromic displays,” *Solid State Ionics*, vol. 292, pp. 8–14, 2016.
- [68] Y. Iida, Y. Kaneko, and Y. Kanno, “Fabrication of pulsed-laser deposited V_2O_5 thin films for electrochromic devices,” *J. Mater. Process. Technol.*, vol. 197, no. 1–3, pp. 261–267, 2008.
- [69] M. Najdoski, V. Koleva, and A. Samet, “Effect of deposition conditions on the electrochromic properties of nanostructured thin films of ammonium intercalated vanadium pentoxide xerogel,” *J. Phys. Chem. C*, vol. 118, no. 18, pp. 9636–9646, 2014.
- [70] M. Buyan, P. A. Brühwiler, A. Azens, G. Gustavsson, R. Karmhag, and C. G. Granqvist, “Facial warming and tinted helmet visors,” *Int. J. Ind. Ergon.*, vol. 36, no. 1, pp. 11–16, 2006.
- [71] L. C. Chen and K. C. Ho, “Design equations for complementary electrochromic devices: Application to the tungsten oxide -Prussian blue system,” *Electrochim. Acta*, vol. 46, no. 13–14, pp. 2151–2158, 2001.
- [72] Y. Chen, Z. Bi, X. Li, X. Xu, S. Zhang, and X. Hu, “High-Coloration Efficiency Electrochromic Device Based on Novel Porous TiO_2 @Prussian Blue Core-Shell Nanostructures,” *Electrochim. Acta*, vol. 224, pp. 534–540, 2017.
- [73] J. Scarminio, A. Talledo, A. A. Andersson, S. Passerini, and F. Decker, “Stress and electrochromism induced by Li insertion in crystalline and amorphous V_2O_5 thin film electrodes,” *Electrochim. Acta*, vol. 38, no. 12, pp. 1637–1642, 1993.
- [74] Y. Shimizu, K. Nagase, N. Miura, and N. Yamazoe, “New preparation process of V_2O_5 thin film based on spin-coating from organic vanadium solution,” *Jpn. J. Appl. Phys.*, vol. 29, no. 9, pp. L1708–L1711, 1990.

- [75] Z. Zhan, J. Cao, W. Xie, L. Hou, Q. Ye, and P. Liu, "Role of vanadium pentoxide hole-extracting nanolayer in rubrene/C₇₀-based small molecule organic solar cells," *J. Nanomater.*, vol. 2014, pp. 2–9, 2014.
- [76] D. Wang, N. K. Elumalai, M. A. Mahmud, M. Wright, M. B. Upama, K. H. Chan and A. Uddin, "V₂O₅-PEDOT: PSS bilayer as hole transport layer for highly efficient and stable perovskite solar cells," *Org. Electron.*, vol. 53, no. May 2017, pp. 66–73, 2018.
- [77] Z. Liu, T. He, H. Wang, X. Song, H. Liu, J. Yang and H. Ma, "Improving the stability of the perovskite solar cells by V₂O₅ modified transport layer film," *RSC Adv.*, vol. 7, no. 30, pp. 18456–18465, 2017.
- [78] J. B. Bates, N. J. Dudney, G. R. Gruzalski, R. A. Zuhr, A. Choudhury, C. F. Luck and J. D. Robertson, "Fabrication and characterization of amorphous lithium electrolyte thin films and rechargeable thin-film batteries," *J. Power Sources*, vol. 43, no. 1–3, pp. 103–110, 1993.
- [79] M. Baba, N. Kumagai, N. Fujita, K. Ohta, K. Nishidate, S. Komaba and B. Kaplan, "Fabrication and electrochemical characteristics of all-solid-state lithium-ion rechargeable batteries composed of LiMn₂O₄ positive and V₂O₅ negative electrodes," *J. Power Sources*, vol. 97–98, pp. 798–800, 2001.
- [80] S. H. Lee, P. Liu, C. E. Tracy, and D. K. Benson, "All-solid-state rocking chair lithium battery on a flexible Al substrate," *Electrochem. Solid-State Lett.*, vol. 2, no. 9, pp. 425–427, 1999.
- [81] N. J. Dudney and B. J. Neudecker, "Solid state thin-film lithium battery systems," *Curr. Opin. Solid State Mater. Sci.*, vol. 4, no. 5, pp. 479–482, 1999.
- [82] A. Šurca and B. Orel, "IR spectroscopy of crystalline V₂O₅ films in different stages of lithiation," *Electrochim. Acta*, vol. 44, no. 18, pp. 3051–3057, 1999.
- [83] S. Beke, S. Giorgio, L. Korösi, L. Nánai, and W. Marine, "Structural and optical properties of pulsed laser deposited V₂O₅ thin films," *Thin Solid Films*, vol. 516, no. 15, pp. 4659–4664, 2008.
- [84] G. J. Fang, Z. L. Liu, Y. Q. Wang, H. H. Liu, and K. L. Yao, "Orientated growth of V₂O₅ electrochromic thin films on transparent conductive glass by pulsed excimer laser ablation technique," *J. Phys. D. Appl. Phys.*, vol. 33, no. 23, pp. 3018–3021, 2000.
- [85] L. Zhao, L. Miao, S. Tanemura, J. Zhou, L. Chen, X. Xiao and G. Xu, "A low

- cost preparation of VO₂ thin films with improved thermochromic properties from a solution-based process,” *Thin Solid Films*, vol. 543, pp. 157–161, 2013.
- [86] C. V. Ramana, O. M. Hussain, B. S. Naidu, and P. J. Reddy, “Spectroscopic characterization of electron-beam evaporated V₂O₅ thin films,” *Thin Solid Films*, vol. 305, no. 1–2, pp. 219–226, 1997.
- [87] D. Vernardou, P. Paterakis, H. Drosos, E. Spanakis, I. M. Povey, M. E. Pemble, and N. Katsarakis, “A study of the electrochemical performance of vanadium oxide thin films grown by atmospheric pressure chemical vapor deposition,” *Sol. Energy Mater. Sol. Cells*, vol. 95, no. 10, pp. 2842–2847, 2011.
- [88] D. Vernardou, E. Spanakis, N. Katsarakis, and E. Koudoumas, “Electrodeposition of V₂O₅ using ammonium metavanadate at room room temperature,” *Adv. Mater. Lett.*, vol. 5, no. 10, pp. 569–572, 2014.
- [89] S. H. Lee, H. M. Cheong, M. J. Seong, P. Liu, C. E. Tracy, A. Mascarenhas and S. K. Deb, “Raman spectroscopic studies of amorphous vanadium oxide thin films,” *Solid State Ionics*, vol. 165, no. 1–4, pp. 111–116, 2003.
- [90] C. Julien, G. A. Nazri, and O. Bergström, “Raman Scattering Studies of Microcrystalline V₆O₁₃,” *Phys. Status Solidi*, vol. 201, no. 1, p. 319, 1997.
- [91] I. E. Wachs, J. M. Jehng, and F. D. Hardcastle, “The interaction of V₂O₅ and Nb₂O₅ with oxide surfaces,” *Solid State Ionics*, vol. 32–33, no. PART 2, pp. 904–910, 1989.
- [92] J. C. Soc, “2322 (A), 1969 Oxide Phonon Spectra 1-67 A,” no. 2322, pp. 2322–2327, 1969.
- [93] C. V. Ramana, R. J. Smith, O. M. Hussain, M. Massot, and C. M. Julien, “Surface analysis of pulsed laser-deposited V₂O₅ thin films and their lithium intercalated products studied by Raman spectroscopy,” *Surf. Interface Anal.*, vol. 37, no. 4, pp. 406–411, 2005.
- [94] J. Mendialdua, R. Casanova, and Y. Barbaux, “XPS studies of V₂O₅, V₆O₁₃, VO₂ and V₂O₃,” *J. Electron Spectros. Relat. Phenomena*, vol. 71, no. 3, pp. 249–261, 1995.
- [95] G. A. Sawatzky and D. Post, “X-ray photoelectron and Auger spectroscopy study of some vanadium oxides,” *Phys. Rev. B*, vol. 20, no. 4, pp. 1546–1555, 1979.

- [96] M. Demeter, M. Neumann, and W. Reichelt, "Mixed-valence vanadium oxides studied by XPS," *Surf. Sci.*, vol. 454, no. 1, pp. 41–44, 2000.
- [97] G. Silversmit, D. Depla, H. Poelman, G. B. Marin, and R. De Gryse, "Determination of the V2p XPS binding energies for different vanadium oxidation states (V5+ to V0+)," *J. Electron Spectros. Relat. Phenomena*, vol. 135, no. 2–3, pp. 167–175, 2004.
- [98] G. Beamson, N. Moslemzadeh, P. Weightman, and J. F. Watts, "Al K α and Cu K α 1 excited XPS of vanadium oxide and VF $_3$ powders: Measurement of the V 1s - KLL Auger parameters," *J. Electron Spectros. Relat. Phenomena*, vol. 162, no. 1, pp. 19–24, 2008.
- [99] C. G. Granqvist, "Handbook of inorganic electrochromic materials". *Elsevier*, pp. 9-13, 1995.
- [100] BILIGIRI, Suresh. Coating thickness measurement challenges using XRF technology. *Metal finishing*, vol.105, no.10, pp. 33-36, 2007.
- [101] W. Giurlani, E. Berretti, M. Innocenti, and A. Lavacchi, "Coating thickness determination using X-ray Fluorescence spectroscopy: Monte Carlo simulations as an alternative to the use of standards," *Coatings*, vol. 9, no. 2, 2019.
- [102] M. M. Margoni, S. Mathuri, K. Ramamurthi, R. R. Babu, and K. Sethuraman, "Sprayed vanadium pentoxide thin films: Influence of substrate temperature and role of HNO $_3$ on the structural, optical, morphological and electrical properties," *Appl. Surf. Sci.*, vol. 418, no. October, pp. 280–290, 2017.
- [103] K. Jeyalakshmi, S. Vijayakumar, S. Nagamuthu, and G. Muralidharan, "Effect of annealing temperature on the supercapacitor behaviour of β - V $_2$ O $_5$ thin films," *Mater. Res. Bull.*, vol. 48, no. 2, pp. 760–766, 2013.
- [104] Z. Wang, J. Chen, and X. Hu, "Electrochromic properties of aqueous sol-gel derived vanadium oxide films with different thickness," *Thin Solid Films*, vol. 375, no. 1–2, pp. 238–241, 2000.
- [105] M. Benmoussa, A. Outzourhit, A. Bennouna, and E. L. Ameziane, "Electrochromism in sputtered V $_2$ O $_5$ thin films: Structural and optical studies," *Thin Solid Films*, vol. 405, no. 1–2, pp. 11–16, 2002.
- [106] S. Komaba, "Functional binders for reversible lithium intercalation into graphite in propylene carbonate and ionic liquid media," *J. Power Sources*, vol.

195, no. 18, pp. 6069–6074, 2010